12-7-2017

Bone Marrow Myeloid Cells Regulate Myeloid-Biased Hematopoietic Stem Cells via a Histamine-Dependent Feedback Loop

Xiaowei Chen
Columbia University Irving Medical Center

Huan Deng
Columbia University Irving Medical Center

Michael J. Churchill
Columbia University Irving Medical Center

Larry L. Luchsinger
Columbia University Irving Medical Center

Xing Du
Columbia University Irving Medical Center

See next page for additional authors

Article

Cell Stem Cell

Bone Marrow Myeloid Cells Regulate Myeloid-Biased Hematopoietic Stem Cells via a Histamine-Dependent Feedback Loop

Graphical Abstract

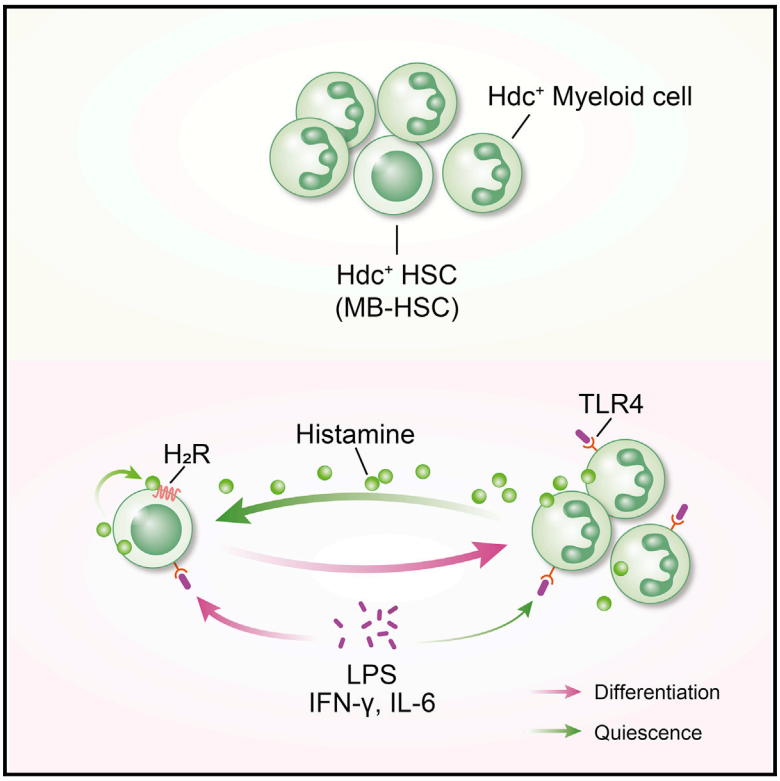

Authors

Xiaowei Chen, Huan Deng, Michael J. Churchill, ..., Hans-Willem Snoeck, Siddhartha Mukherjee, Timothy C. Wang

Correspondence

sm3252@columbia.edu (S.M.), tcw21@columbia.edu (T.C.W.)

In Brief

Chen et al. show that histidine decarboxylase (Hdc) marks quiescent myeloid-biased HSCs (MB-HSCs). Daughter myeloid cells form a spatial cluster with Hdc$^+$ MB-HSCs and secrete histamine to enforce their quiescence and protect them from depletion, following activation by a variety of physiologic insults.

Highlights

- Hdc marks a population of myeloid-biased HSCs and progenitors
- Hdc$^+$ MB-HSCs specifically respond to physiological insults demanding myeloid output
- Hdc$^+$ myeloid cells within the BM secrete histamine that activates H_2R on MB-HSCs
- A histaminergic circuit restores quiescence and protects MB-HSCs from depletion

Chen et al., 2017, Cell Stem Cell *21*, 747–760
December 7, 2017 Published by Elsevier Inc.
https://doi.org/10.1016/j.stem.2017.11.003

Cell Stem Cell
Article

Bone Marrow Myeloid Cells Regulate Myeloid-Biased Hematopoietic Stem Cells via a Histamine-Dependent Feedback Loop

Xiaowei Chen,[1,2,3,20] Huan Deng,[1,2,3,4,20] Michael J. Churchill,[2] Larry L. Luchsinger,[5,6] Xing Du,[2] Timothy H. Chu,[1,3] Richard A. Friedman,[3,7] Moritz Middelhoff,[1,3] Hongxu Ding,[7,8] Yagnesh H. Tailor,[1,3] Alexander L.E. Wang,[1,3] Haibo Liu,[1,3] Zhengchuan Niu,[1,3,9] Hongshan Wang,[1,3,9] Zhengyu Jiang,[1,3] Simon Renders,[2,10] Siu-Hong Ho,[5] Spandan V. Shah,[5] Pavel Tishchenko,[5] Wenju Chang,[1,3,9] Theresa C. Swayne,[3] Laura Munteanu,[3] Andrea Califano,[7,8] Ryota Takahashi,[1,3] Karan K. Nagar,[1,3] Bernhard W. Renz,[1,3,11] Daniel L. Worthley,[1,3,12,13] C. Benedikt Westphalen,[1,3,14] Yoku Hayakawa,[1,3,15] Samuel Asfaha,[1,3,16] Florence Borot,[2] Chyuan-Sheng Lin,[3,17] Hans-Willem Snoeck,[5,6,18,19] Siddhartha Mukherjee,[2,*] and Timothy C. Wang[1,3,21,*]

[1]Division of Digestive and Liver Disease, Department of Medicine, Columbia University Medical Center, New York, NY 10032, USA
[2]Division of Hematology/Oncology, Department of Medicine, Columbia University Medical Center, New York, NY 10032, USA
[3]Herbert Irving Comprehensive Cancer Center, Columbia University Medical Center, New York, NY 10032, USA
[4]Department of Pathology and Molecular Medicine and Genetics Center, The Fourth Affiliated Hospital of Nanchang University, Nanchang, Jiangxi 330003, China
[5]Columbia Center for Translational Immunology, Columbia University Medical Center, New York, NY 10032, USA
[6]Center for Human Development, Columbia University Medical Center, New York, NY 10032, USA
[7]Biomedical Informatics Shared Resource, Herbert Irving Comprehensive Cancer Center, and Department of Biomedical Informatics, Columbia University Medical Center, New York, NY 10032, USA
[8]Department of Systems Biology, Columbia University, New York, NY 10032, USA
[9]Department of General Surgery, Zhongshan Hospital, Fudan University, Shanghai 200032, China
[10]Division of Stem Cells and Cancer, German Cancer Research Center (DKFZ), DKFZ-ZMBH Alliance and Heidelberg Institute for Stem Cell Technology and Experimental Medicine (HI-STEM gGmbH), 69120 Heidelberg, Germany
[11]Department of General, Visceral and Transplantation Surgery, Hospital of the University of Munich, 81377 Munich, Germany
[12]School of Medicine, University of Adelaide, Adelaide, SA 5005, Australia
[13]Cancer Theme, SAHMRI, Adelaide, SA 5005, Australia
[14]Department of Medicine III, University Hospital, LMU Munich, 81377 Munich, Germany
[15]Department of Gastroenterology, Graduate School of Medicine, the University of Tokyo, 7-3-1, Hongo, Bunkyo-ku, Tokyo 113-8655, Japan
[16]Department of Medicine, University of Western Ontario, London, ON N6A 5W9, Canada
[17]Department of Pathology and Cell Biology, Columbia University Medical Center, New York, NY 10032, USA
[18]Department of Medicine, Columbia University Medical Center, New York, NY 10032, USA
[19]Department of Microbiology and Immunology, Columbia University Medical Center, New York, NY 10032, USA
[20]These authors contributed equally
[21]Lead Contact
*Correspondence: sm3252@columbia.edu (S.M.), tcw21@columbia.edu (T.C.W.)
https://doi.org/10.1016/j.stem.2017.11.003

SUMMARY

Myeloid-biased hematopoietic stem cells (MB-HSCs) play critical roles in recovery from injury, but little is known about how they are regulated within the bone marrow niche. Here we describe an auto-/paracrine physiologic circuit that controls quiescence of MB-HSCs and hematopoietic progenitors marked by histidine decarboxylase (Hdc). Committed Hdc^+ myeloid cells lie in close anatomical proximity to MB-HSCs and produce histamine, which activates the H_2 receptor on MB-HSCs to promote their quiescence and self-renewal. Depleting histamine-producing cells enforces cell cycle entry, induces loss of serial transplant capacity, and sensitizes animals to chemotherapeutic injury. Increasing demand for myeloid cells via lipopolysaccharide (LPS) treatment specifically recruits MB-HSCs and progenitors into the cell cycle; cycling MB-HSCs fail to revert into quiescence in the absence of histamine feedback, leading to their depletion, while an H_2 agonist protects MB-HSCs from depletion after sepsis. Thus, histamine couples lineage-specific physiological demands to intrinsically primed MB-HSCs to enforce homeostasis.

INTRODUCTION

Adult bone marrow (BM) hematopoietic stem cells (HSCs) are typically maintained in a quiescent state and demonstrate regenerative capacity after injury (Trumpp et al., 2010). For decades, hematopoiesis in either homeostatic or regenerative conditions was thought to transpire in a cascade-like manner with progressive lineage commitment, a process that was postulated to originate in a population of self-renewing and multipotent HSCs, which were believed to give rise proportionally to multiple

lineage-committed progenitors and further differentiate into myeloid or lymphoid descendants.

However, recent studies indicate that HSCs are heterogeneous and vary in their capacity for self-renewal and lineage output (Dutta et al., 2015; Morita et al., 2010; Sanjuan-Pla et al., 2013). Among the primitive adult BM HSC compartments, myeloid-biased HSCs (MB-HSCs) exhibit greater self-renewal and long-term (LT) repopulation capability (Morita et al., 2010). Although the rapid response by myeloid cells to tissue inflammation and injury requires a relatively dynamic BM myeloid pool, MB-HSCs are paradoxically more quiescent than the rest of HSCs (Challen et al., 2010; Land et al., 2015). Furthermore, biased lineage differentiation is exaggerated in the setting of inflammation (Dutta et al., 2015). The notion of lineage-biased activation of HSCs suggests that lineage-specific demands in an organism may initiate the recruitment of lineage-committed progenitors (e.g., myeloid progenitors after bacterial infection), but lineage-biased HSCs may also be differentially recruited, thereby coordinating an organism's demands for regeneration at the stem cell level (King and Goodell, 2011). Whether this process occurs and how such a system might be restored to homeostasis remain important questions in HSC biology.

The self-renewal and lineage commitment properties of HSCs can be engendered and regulated by either intrinsic cellular properties or extrinsic niche factors. Niche cells are thought to impose stem cell features on daughter cells, restrict stem cell proliferation, and integrate signals reflecting organismal state. In addition to well-studied stromal niche cells (Morrison and Scadden, 2014), hematopoietic lineage descendants have been reported to promote HSC retention (Bruns et al., 2014; Zhao et al., 2014). Although this hypothesis fits well in a model of dynamic niche regulation, little is known as to how niche daughters regulate lineage-biased HSCs. Nevertheless, recent studies have suggested that MB- and lymphoid-biased (LB-) HSCs and progenitors respond differentially to niche factors (Challen et al., 2010; Cordeiro Gomes et al., 2016), indicating that lineage-biased HSCs and progenitors might reside in distinct niches and be differentially regulated by specific demands.

The stem cell niche is thought to be critical for sustaining the dormancy of HSCs, which must limit their divisions in order to maintain a steady-state pool of self-renewing HSCs. In the setting of acute infection or injury, myeloid cells quickly traffic out of BM, followed by a rapid increase in the proliferation of MB-HSCs and progenitors. However, if this acute myeloid demand is not resolved, the prolonged entry of HSCs into the cell cycle can lead to HSC depletion (Trumpp et al., 2010). Thus, current studies on MB-HSCs have raised several crucial questions. First, what regulates intrinsically biased HSCs in their native niche to keep them in dormancy during homeostasis? Second, how does the HSC and progenitor regulatory network coordinate in regard to lineage-specific demands of an organism? Third, how does this regulatory network restore homeostasis?

The histamine-synthesizing enzyme histidine decarboxylase (Hdc) is highly expressed in both human and mouse myeloid lineages, and it has been used as a marker to track myeloid cell fate (Terskikh et al., 2003). Furthermore, Hdc in myeloid cells is primarily responsible for histamine production in acute and chronic inflammation, where it plays a role in suppressing myeloid proliferation and inflammation (Brune et al., 2006; Yang et al., 2011). However, it has not been established precisely how histamine signals are integrated by the HSCs and progenitors and whether Hdc gene expression is part of the early transcriptional priming of the myeloid lineage. Here we provide evidence for a previously unknown regulatory circuit, driven by the myeloid lineage-specific auto-/paracrine factor histamine, which is mainly produced by myeloid descendants and feeds back on MB-HSCs and progenitors to maintain their quiescence and protect them from myelotoxic injury and depletion.

RESULTS

Hdc Expression Identifies MB-HSC and Myeloid Lineage

We examined Hdc expression in BM primitive and differentiated cells in Hdc-GFP mice (Figures 1A and 1B). Consistent with their heterogeneous nature, a continuum of Hdc-GFP expression was observed in HSCs and progenitors (Figures 1A and S1B) (Morita et al., 2010). Small subsets of HSCs (10.3% ± 2.27%) and progenitors (14.33% ± 2.17%), as well as the vast majority of granulocyte-macrophage progenitors (GMPs) and myeloid cells, expressed high levels of Hdc-GFP (henceforth referred to as Hdc-GFP^{hi} and Hdc-GFP^{lo}) (Figures 1B, S1B, and S1C) (Yang et al., 2011).

Hdc-GFP expression was detected in macrophage dendritic cell progenitors (MDPs) and common dendritic cell precursors (CDPs) (Figure S1D). Common lymphoid progenitors (CLPs) and other lymphoid lineages of cells, however, lacked Hdc-GFP expression (Figure S1E). Few BM stromal cells expressed Hdc-GFP (Figure S1F). The Hdc mRNA level was higher in erythrocytes compared to T and B cells, consistent with the greater relative expression in their progenitors. However, these levels were much lower than that seen in myeloid cells (Figure 1B). Among all Hdc-GFP-expressing cells, CD11b^{+}Gr1$^{+/hi}$ granulocytic myeloid cells expressed the highest level of Hdc mRNA (Figures 1B and S2A). To exclude any insertional effects of the Hdc-GFP BAC transgene, we compared wild-type (WT) and Hdc-GFP mice, and we noted similar levels of Hdc mRNA expression, histamine, and cytokines in hematopoietic lineages (Figures S1G–S1I) (Table S1).

Aging is known to influence the top of the hematopoietic hierarchy, and it contributes to the myeloid-biased behaviors of HSCs (Beerman et al., 2010), most likely through effects on the relative number of MB-HSCs (Challen et al., 2010). Thus, we investigated the absolute numbers of myeloid lineage cells from young (4-month-old) and aged (16-month-old) WT and Hdc-GFP mice. Consistent with mRNA results (Figures S1G–S1I), the Hdc-GFP transgene did not affect the numbers of BM HSCs, hematopoietic stem and progenitor cells (HSPCs), GMPs, blood myeloid cells, and lymphocytes (Figures 1D, S1J, and S1K). However, the percentage and absolute number of HSCs from aged mice increased significantly compared to young mice (Figure 1C). Thus, to minimize age-related bias in our studies, we primarily used young mice (<4 months) and littermates.

Both perivascular cells and vascular endothelial cells can express Cxcl12 in BM (Ding and Morrison, 2013). Histologic analysis showed that Hdc-GFP-expressing cells were situated immediately adjacent to Cxcl12^{+} perivascular stromal cells and

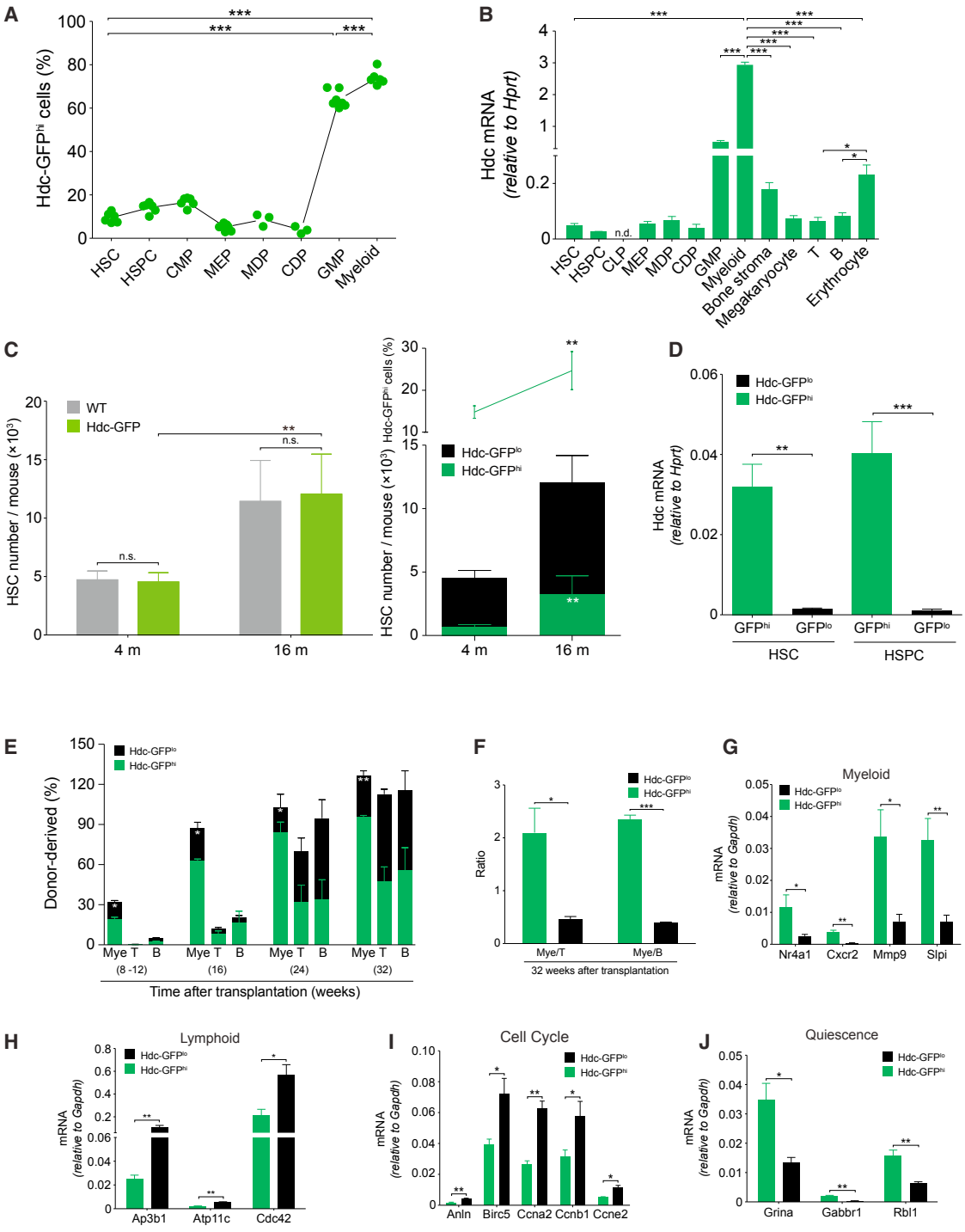

Figure 1. Hdc Expression Identifies MB-HSCs

(A) Percentage of Hdc-GFP^{hi} cells in lineages of bone marrow (BM) cells (n = 3–7 per group; six independent experiments).

(B) mRNA expression of Hdc gene in BM cells and stromal cells (n = 3–5).

(C) Quantification of Hdc-GFP^{hi} HSCs in Hdc-GFP and WT mice (n = 3 per group).

(D) Hdc mRNA expression in Hdc-GFP^{hi} and Hdc-GFP^{lo} BM HSCs and HSPCs (n = 3 per group).

(E) Contribution of Hdc-GFP^{hi} HSCs (n = 12) to lethally irradiated recipients.

(F) Blood myeloid/lymphoid ratio of recipients in (E).

(G–J) Relative mRNA expression of myeloid (G) and lymphoid lineage (H), cell cycle (I), and quiescence signatures genes (J) in HSCs (n = 3–4 per group). Data were analyzed with one-way ANOVA with Bonferroni post hoc test (A and B) or two-tailed Student's t test (C–J). See also Figures S1–S3.

Laminin^{+} vascular matrix, but they rarely overlapped with these stromal elements (Figures S1L and S1M).

Sorted Hdc-GFP^{hi} HSCs showed greater myeloid colony-forming unit (CFU) potential than Hdc-GFP^{lo} counterparts (Figure S2B). Within common myeloid progenitors (CMPs) and GMPs, Hdc-GFP^{hi} cells also generated more myeloid colonies, especially granulocytic colonies (Figure S2C), indicating a granulocytic bias in Hdc-GFP^{hi} progenitors. Moreover, single Hdc-GFP^{hi} HSCs tended to form larger and denser single-myeloid colonies compared to Hdc-GFP^{lo} HSCs (Figure S2D), which was not surprising given that the culture medium was optimized for growth of primitive myeloid progenitor cells. In contrast to their increased myeloid output, under pre-B colony formation conditions, Hdc-GFP^{hi} HSPCs formed fewer B colonies, leading to a higher myeloid/B ratio with Hdc-GFP^{hi} HSPCs compared to that with Hdc-GFP^{lo} counterparts (Figure S2E). These data suggest a distinct *in vitro* myeloid bias for Hdc-GFP^{hi} HSCs and progenitors.

We performed additional cell culture experiments to investigate the stability of Hdc-GFP^{hi}. After cultured for 5 days, a minority (5.67% ± 1.76%) of Hdc-GFP^{lo} cells were detected in the Hdc-GFP^{hi} HSC group, but not vice versa (Figure S2F). To compare the multilineage reconstitution ability of Hdc-GFP^{hi} and Hdc-GFP^{lo} HSCs, we serially transplanted sorted Hdc-GFP^{hi} and Hdc-GFP^{lo} HSCs into lethally irradiated recipients, along with 2 × 10^5 CD45.1^{+} competitor BM cells (Figure S2G). Notably, the transplantation of 20 Hdc-GFP^{hi} HSCs yielded robust myeloid chimerism, with greater than 2-fold more myeloid cells in the peripheral blood of recipients at 32 weeks (Figure 1E). In addition, the donor-derived myeloid/lymphoid ratio was significantly higher than that in recipients of Hdc-GFP^{lo} HSCs (Figure 1F). Even at 1 year after transplantation, the myeloid bias of Hdc-GFP^{hi} donor cells was maintained (Figure S2H). Notably, Hdc-GFP^{hi} HSCs had greater blood donor and myeloid chimerism (Figures S2I and S2J). This effect persisted in secondary transplants, with skewing of donor myeloid/lymphoid ratio at 16 weeks, similar to that seen in the primary transplant (Figures S2K and S2L). Although there was less myeloid bias in secondary transplants with Hdc-GFP^{hi} HSCs, it was still much greater than that with Hdc-GFP^{lo} HSCs.

A similar myeloid bias was observed in mice transplanted with 50 Hdc-GFP^{hi} HSCs (Figure S2M). Serial transplantation studies, using 20 or 50 HSCs, revealed some degree of reconstitution of myeloid and lymphoid lineages with both types of HSCs (Figure S2N). However, Hdc-GFP^{hi} HSCs showed a higher myeloid lineage reconstitution and a lower lymphoid reconstitution in limiting dilution assays or by the percentage of responders. In single-cell transplantations with Hdc-GFP^{hi} or Hdc-GFP^{lo} HSCs ($n > 40$ per group), limited HSC reconstitution was observed, but Hdc-GFP^{hi} HSCs indeed showed a greater myeloid lineage repopulation potential and a higher myeloid/lymphoid reconstitution ratio (Figure S2O).

We performed a transcriptome analysis to characterize the Hdc-GFP^{hi} HSCs. In total, 748 genes were significantly upregulated while 1,149 genes were downregulated ($p < 0.05$, false discovery rate [FDR] < 0.28). Myeloid-specific genes and quiescence regulators were expressed at higher levels (Figure 1G) (Table S1) (Ardi et al., 2007; Klimenkova et al., 2014; Land et al., 2015; Schinke et al., 2015), whereas lymphoid-specific, cell cycle, DNA replication, and mitochondrial function genes were downregulated in Hdc-GFP^{hi} HSCs (Figures 1H–1J and S2P) (Table S1) (Cheung and Rando, 2013; Guo et al., 2009; Jung et al., 2006; Siggs et al., 2011; Viatour et al., 2008). These results are consistent with the observed myeloid bias and quiescence of Hdc-GFP^{hi} HSCs. Moreover, Hdc-GFP^{hi} HSCs preferentially expressed lower Dpp4 but higher Ogt (Figure S2Q) (Table S1) (Broxmeyer et al., 2012; Hart et al., 2011), suggesting that MB-HSCs may be resistant to stress. Similar signatures were also observed in Hdc-GFP^{hi} HSPCs (Figures S3A and S3B). Taken together, the gene expression patterns support the heterogeneity of HSCs and progenitors, which can be divided into two categories (MB Hdc-GFP^{hi} and LB Hdc-GFP^{lo}) by Hdc-GFP expression.

Myeloid Demand Stimuli Activate Hdc-GFP^{hi} MB-HSCs

Acute bacterial infection induces the production and mobilization of myeloid cells. Toll-like receptors (TLRs) expressed on myeloid cells are known to sense bacterial products, which lead to rapid myelopoiesis (Nagai et al., 2006; Takeuchi et al., 1999). Lipopolysaccharide (LPS) treatment recapitulates gram-negative bacterial infection, and it specifically activates TLR4 on myeloid cells (Takizawa et al., 2017). HSCs can be activated by LPS either directly through cell-intrinsic TLR signaling or indirectly through the upregulation of myeloid-derived inflammatory cytokines (Nagai et al., 2006; Rodriguez et al., 2009).

We found that Hdc-GFP^{hi} HSCs and myeloid cells expressed higher levels of TLR4 compared to Hdc-GFP^{lo} counterparts (Figure 2A) (Table S1). In particular, TLR2/4/6 genes were highly enriched in granulocytic myeloid cells (Figures 2B and S3C) (Table S1) (Chen et al., 2017). As LPS elicits histamine release from Hdc-expressing cells (Alcañiz et al., 2013), we analyzed histamine release from Hdc-GFP^{hi} HSCs and myeloid cells in response to *in vitro* LPS stimulation. The results showed that only Hdc-GFP^{hi} myeloid cells were capable of releasing a large amount of histamine shortly after LPS treatment (Figure S3D), indicating that Hdc-expressing myeloid cells preferentially sense and respond to bacteria-mediated TLR signals.

Next, we injected LPS intravenously into Hdc-GFP mice and quantified HSCs and progenitors. Hdc-GFP^{hi} HSCs, but not myeloid cells, transiently increased at 6 hr (Figure 2C), consistent with LPS-induced myeloid demand (Nagai et al., 2006; Rodriguez et al., 2009). LPS treatment induced an increase in BM Hdc-GFP^{hi} myeloid cells, along with a sharp decrease of Hdc-GFP^{hi} HSCs (Figure 2C) and in the proliferation and frequencies of splenic myeloid cells and progenitors at 24 hr (Figures 2D–2F and S3E). Taken together, these data suggest that myeloid demand promotes the early differentiation of Hdc-GFP^{hi} HSCs and progenitors into myeloid cells to replenish the LPS-induced emergency myeloid consumption.

In line with this observation, cell cycle analysis showed that Hdc-GFP^{hi} HSCs, but not Hdc-GFP^{lo} HSCs, lost quiescence as early as 6 hr after LPS treatment (Figures 2E and 2F). Analysis of PBS-treated controls confirmed earlier observations that Hdc-GFP^{hi} HSCs showed essentially no proliferation under basal conditions (Figures 1I, 1J, and S2P). A previous study suggested that the TLR4/Sca-1 axis contributes to granulopoiesis in the setting of bacterial infection or LPS treatment (Shi et al., 2013). While Sca-1 expression in Lin^{-}c-kit^{+}Sca-1^{-} cells was upregulated

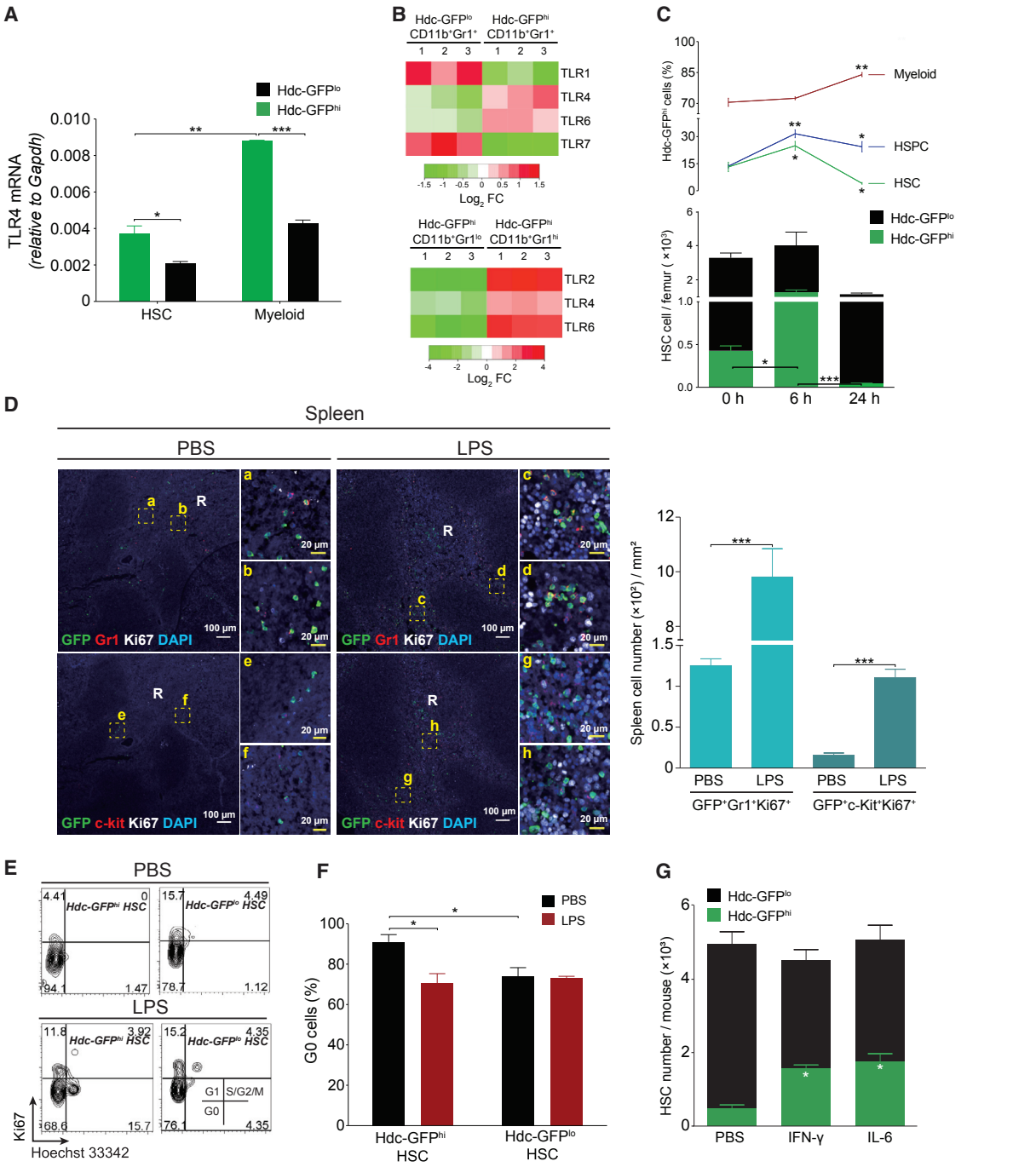

Figure 2. Myeloid Stimuli Activate Hdc-GFP^{hi} MB-HSCs

(A) TLR4 mRNA in HSCs (n = 3–4) and myeloid cells (n = 5).

(B) TLR expression from gene microarray analysis in myeloid cells (n = 3 per group).

(C) Quantification of HSCs, HSPCs, and myeloid cells at 24 hr after LPS treatment (n = 5).

(D) Myeloid cells (Gr1$^+$) and progenitors (c-kit$^+$) in spleen from LPS- (n = 4) or PBS- (n = 3) treated Hdc-GFP mice (four independent experiments).

(E and F) Cell cycle analysis with FACS for Ki67$^+$ cells (A) and quantitation of G0 cells (B) of BM HSCs at 6 hr after PBS (n = 3) or LPS (n = 3) treatment.

(G) Absolute numbers of HSCs in BM of Hdc-GFP mice treated with PBS, IFN-γ, or IL-6 (n = 5 per group). Data were analyzed with two-tailed Student's t test (A, F, and G) or one-way ANOVA with Bonferroni post hoc test (C). See also Figure S3.

slightly in response to LPS *in vitro*, the expansion of HSPCs *in vivo* was due primarily to an increase in Lin$^-$c-kit$^+$Sca-1$^+$ cells. Although Hdc-GFP^{lo} HSCs were less affected at 6 hr, they showed a significant decrease at 24 hr, suggesting that LPS-induced depletion of Hdc-GFP^{hi} HSCs may also stimulate the differentiation of Hdc-GFP^{lo} HSCs (Figures 2C, 3E, and S3E).

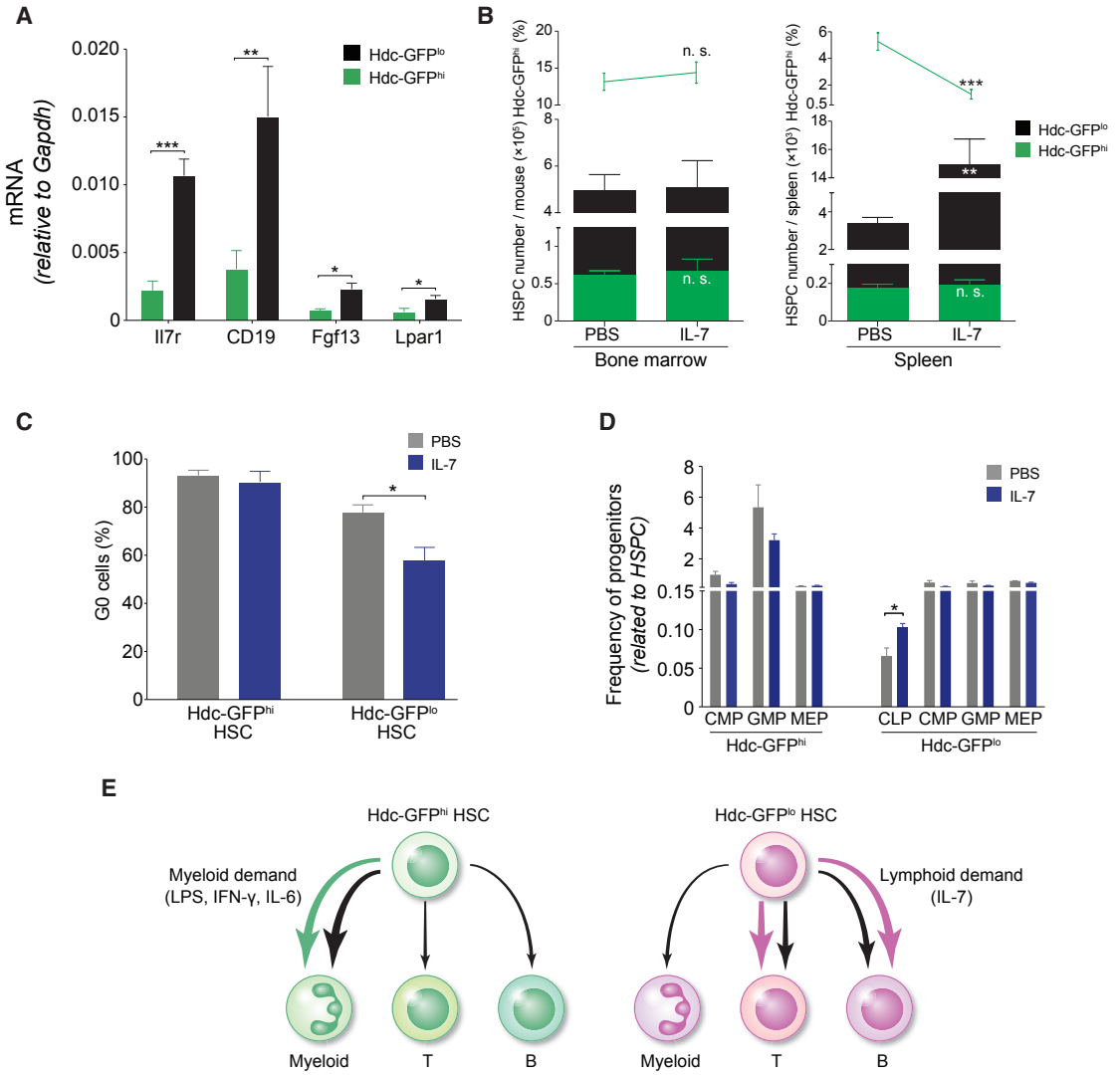

Figure 3. Hdc-GFP^{hi} MB-HSCs Are Not Responsive to IL-7

(A) Relative mRNA expression of IL-7/IL-7R pathway genes in HSPCs (n = 4 per group).

(B) Quantification of Hdc-GFP^{hi} HSPCs in IL-7- or PBS-treated mice (n = 3 per group).

(C) Percentage of G0 HSCs (n = 3 per group).

(D) Frequencies of progenitors in IL-7- or PBS-treated Hdc-GFP mice (n = 5 per group).

(E) Schematic depiction of the relative lineage bias of Hdc-GFP^{hi} HSCs or Hdc-GFP^{lo} HSCs. Data were analyzed with two-tailed Student's t test (A–D). See also Figure S3.

Interferon (IFN)-γ can activate LT-HSCs, leading to myeloid differentiation (de Bruin et al., 2012), and it can promote BM stromal cells to secret interleukin (IL)-6, which in turn increases myeloproliferation through the inhibition of *Runx-1* and *Cebpα* in HSCs (Schürch et al., 2014). We intravenously injected Hdc-GFP mice with recombinant mouse IFN-γ or IL-6 to test the responsiveness of Hdc-GFP^{hi} HSCs, and we measured absolute numbers of HSCs and progenitors at 48 hr. Sca-1 was excluded because of the nonspecific expression induced by IFN-γ (Matatall et al., 2016). Both IFN-γ and IL-6 exclusively increased MB-HSCs and progenitors (Figures 2G, S3F, and S3G). Taken together, these observations suggest that Hdc-GFP^{hi} MB-HSCs are preferentially activated by myeloid stimulants (see Figure 3E).

Hdc-GFP^{hi} MB-HSCs Are Refractory to Lymphoid Stimulus

We next asked whether Hdc-GFP^{hi} HSCs are refractory to lymphoid stimulus. The IL-7/IL-7Ra axis has been shown to activate and expand lymphocytes and their progenitors (Dias et al., 2005). IL-7/IL7-Ra pathway genes were predominantly expressed in Hdc-GFP^{lo} rather than Hdc-GFP^{hi} HSPCs (Figure 3A; RNA sequencing [RNA-seq], GEO: GSE80092) (Table S1). The injection of IL-7 into Hdc-GFP mice activated Hdc-GFP^{lo} HSPCs, leading to an expansion of Hdc-GFP^{lo} HSPCs in the spleen (Figure 3B). Moreover, IL-7 decreased the proportion of quiescent (G0) Hdc-GFP^{lo} HSCs and increased the output of CLPs (Figures 3C and 3D). In summary, these findings indicate

that Hdc-GFP^{hi} HSCs or HSPCs are not responsive to the lymphoid stimulant (Figure 3E).

Hdc Deficiency Provokes Myeloid Proliferation from MB-HSCs

Given that Hdc-expressing myeloid cells may be a major source of histamine in the BM (Yang et al., 2011), we hypothesized that myeloid-derived histamine could be an important niche factor for maintaining the quiescence and self-renewal of MB-HSCs. The *Hdc*$^{-/-}$ mouse was crossed with the Hdc-GFP mouse. The Hdc-BAC-GFP transgenic mouse contains several transgene copies of a BAC transgene integrated randomly at a single (non-Hdc) chromosomal site, and, thus, mice could be bred into an Hdc-deficient background, yielding *Hdc*$^{-/-}$; Hdc-GFP mice as previously reported (Yang et al., 2011). Hdc-GFP^{hi} *Hdc*$^{-/-}$ HSCs and BM cells showed increased myeloid colony expansion compared to Hdc-GFP^{hi} *Hdc*$^{+/+}$ controls (Figures 4A and 4B), indicating that Hdc and histamine were relatively specific for Hdc-GFP^{hi} MB-HSCs and progenitors. We further found that, while Hdc-GFP^{hi} HSCs were largely quiescent at baseline, Hdc deficiency led to increased proliferation in Hdc-GFP^{hi} *Hdc*$^{-/-}$ HSCs and progenitors (Figures 4C and S4A). Within the BM GFP^{hi}LSK population, the frequencies of MB-HSCs and multi-potent progenitors (MPPs) were decreased, while that of myeloid-biased MPP3 was increased (Figures 4D and 4E). In competitive repopulation experiments, *Hdc*$^{-/-}$ BM cells showed a deficiency in the reconstitution of all lineages, particularly in LT myeloid reconstitution. Although lymphoid reconstitution was also reduced, it was less dramatically affected compared to myeloid cells in the long term, suggesting that Hdc ablation preferentially affected MB-HSCs (Figure 4F). Furthermore, when we transplanted unfractionated *Hdc*$^{-/-}$ BM cells into lethally irradiated WT mice, a similar tendency was observed (Figure S4B).

To test the functional consequence of increased cell cycle entry by *Hdc*$^{-/-}$ MB-HSPCs, we treated *Hdc*$^{-/-}$ mice with 5-fluorouracil (5-FU) to selectively eliminate rapidly cycling MB-HSCs and progenitors. The replenishment of HSCs, HSPCs, and myeloid cells was much more impaired in *Hdc*$^{-/-}$ mice compared to WT (Figures S4C and S4D). Furthermore, *Hdc*$^{-/-}$ mice died significantly earlier than WT littermates (Figure 4G). Transcriptome comparison between WT and *Hdc*$^{-/-}$ HSPCs again confirmed that Hdc deficiency led to the upregulation of proliferative, myeloid, apoptosis-related, and erythroid differentiation transcripts (Figures S4E–S4K) (Table S1). Overall, our results suggest that the enhanced sensitivity of *Hdc*$^{-/-}$ HSCs and progenitors to 5-FU contributes to the early lethality of *Hdc*$^{-/-}$ mice.

Hdc-Expressing Myeloid Cells Maintain MB-HSC Quiescence through the Histamine/H_2R Axis

Dormant HSCs proliferate in response to inflammation, yet they are capable of returning to quiescence once the stimulus resolves (Trumpp et al., 2010). However, specific niche factors that restore homeostasis in a lineage-restricted fashion have not been well defined. We observed that GFP$^+$ MB-HSCs, but not GFP$^-$ LB-HSCs, were located in close anatomical proximity to more than one GFP$^+$ myeloid cell in direct contact, forming a tight cluster (Figures 5A and 5B). The staining with anti-Gr1 antibody showed that 79.80% ± 2.50% of the MB-HSC surrounding cells were GFP$^+$Gr1$^+$ myeloid cells (Figures S5A and S5B). Although GFP$^+$Gr1$^+$ myeloid cells comprise more than 30% of total BM cells (Yang et al., 2011), computational comparison between randomly placed HSCs and GFP$^+$ HSCs revealed that the distribution pattern of GFP$^+$ MB-HSCs within the MB-HSC/myeloid cluster was not random (Figure 5C).

Using Laminin to decorate the BM vascular matrix, we found that 79.45% ± 6.85% of such clusters were located within 5-μm distance of Laminin$^+$ cells (Figures S5C and S5D). Although the pervasive presence of GFP$^+$ myeloid cells makes it difficult to assess precisely the juxtaposition of these cells with MB-HSCs, these staining experiments and simulations demonstrate a preferential apposition between MB-HSCs and histamine-producing myeloid cells.

The clusters suggested that myeloid cells may regulate MB-HSCs through a paracrine feedback. We thus utilized the inducible diphtheria toxin receptor (iDTR) to deplete Hdc-expressing myeloid cells in Hdc-CreER^{T2}; tdTomato; iDTR mice (Figure S5E). Two weeks of tamoxifen-containing diet labeled around 25% of myeloid cells (Figure S5F). Notably, the tamoxifen chow spared HSCs (Figure S5G), and, in accordance, there was no significant change in the numbers of HSCs or HSPCs in DTR$^+$ mice compared to DTR$^-$ groups (Figure S5H). This absence of effects on HSCs and HSPCs was likely due to the low expression levels of CreER^{T2} and iDTR transgene, resulting in a lack of sensitivity to DT (Figures S5I and S5J).

The depletion of Hdc^{hi} myeloid cells decreased BM histamine levels and caused MB-HSCs to lose quiescence, which could be partially rescued by adoptive transfer of *Hdc*$^{+/+}$, but not *Hdc*$^{-/-}$;Hdc-GFP^{hi} myeloid cells (Figures S5K and 5D). Notably, we observed significantly lower donor cell reconstitution over a period of 16 weeks in recipient mice that received donor BM cells from DTR$^+$ mice compared with the DTR$^-$ control group (Figure 5E). Gr1$^+$ depletion induced by the Gr1 monoclonal antibody RB6-8C5 can mimic the activation of emergency myelopoiesis. More than 30% of BM Hdc-GFP^{hi} cells were depleted after RB6-8C5 treatment, and MB-HSCs were induced to enter the cell cycle (Figures S5L and 5F), further surpporting the role of Hdc-GFP^{hi} myeloid cells in maintaining MB-HSC quiescence. In summary, our data suggest that Hdc-GFP^{hi} myeloid cells are spatially located close to MB-HSCs and functionally serve as a critical MB-HSC homeostasis niche component.

We next investigated the mechanism of histamine action on MB-HSCs and progenitors. Among the four known histamine receptors, only H_2R was detectable on both HSCs and progenitors (Figure S5M). Hdc-GFP^{hi} MB-HSCs and progenitors expressed higher levels of H_2R compared to Hdc-GFP^{lo} counterparts (Figure S5N). *H_2R*$^{-/-}$ BM cells exhibited a similar myeloid lineage repopulation defect as *Hdc*$^{-/-}$ BM cells (Figure 5G). Unlike *Hdc*$^{-/-}$ animals, *H_2R*$^{-/-}$ recipients also exhibited significant lymphoid reconstitution defects, which could be due to the compensatory expression of other histamine receptor(s) on *H_2R*$^{-/-}$ HSCs (Saligrama et al., 2012).

The increased expression of H_2R on MB-HSCs and progenitors also raised the possibility that these cells might be intrinsically more responsive to histamine. To test this hypothesis, we co-cultured *Hdc*$^{-/-}$;Hdc-GFP^{hi} HSPCs with *Hdc*$^{-/-}$ BM stromal cells, establishing a culture system lacking endogenous

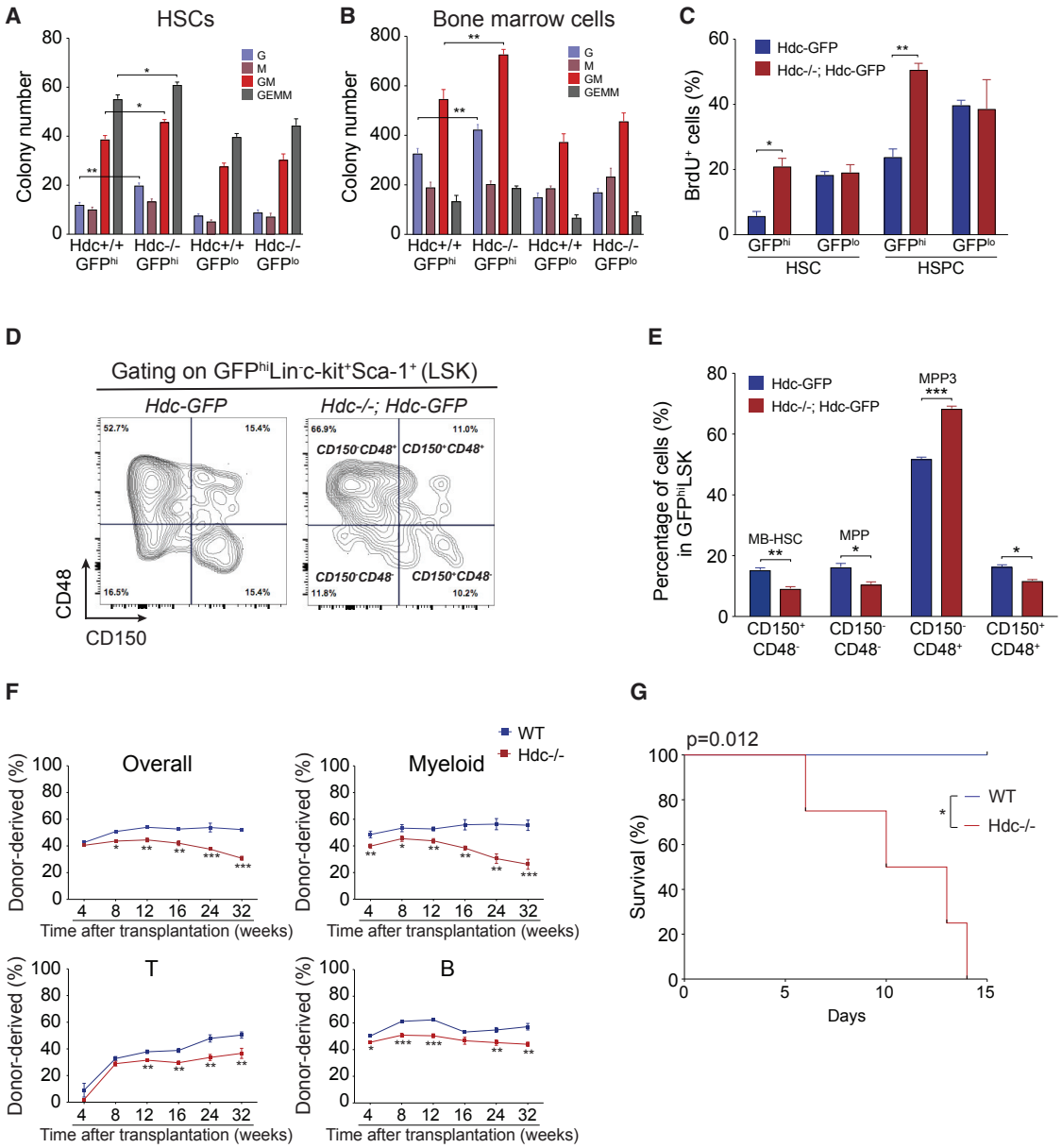

Figure 4. Hdc Deficiency Leads to MB-HSC Activation

(A and B) Absolute numbers of myeloid CFUs from 150 BM HSCs (A) and 1 × 10^5 BM cells (B) (n = 3 per group; three independent experiments).

(C) BrdU incorporation of HSCs and HSPCs (n = 5 per group).

(D and E) Analysis of GFP^{hi} LSK cells from Hdc-GFP and *Hdc*$^{-/-}$; Hdc-GFP mice showing FACS plots (D) and quantitation (E) for MB-HSC (CD150$^+$CD48$^+$) and MPP (CD150$^-$CD48$^-$) and MPP3 (CD150$^-$CD48$^+$).

(F) Competitive transplantation assays of 2 × 10^5 unfractionated BM cells from *Hdc*$^{-/-}$ (n = 12) or WT mice (n = 10).

(G) Kaplan-Meier curve depicting survival rates of *Hdc*$^{-/-}$ (n = 6) and WT mice (n = 5) after 5-FU treatment. Data were analyzed with two-tailed Student's t test (A–C, E, and F) or log rank test (G). See also Figure S4.

histamine. First, we noted that the addition of histamine increased the G0/quiescence frequency in WT and *Hdc*$^{-/-}$ HSPCs, but not *H*$_2$*R*$^{-/-}$ HSPCs (Figure S5O), demonstrating an H_2R-dependent histamine response. Next, the addition of an H_2 agonist (dimaprit dihydrochloride) selectively increased the quiescence of *Hdc*$^{-/-}$ Hdc-GFP^{hi} HSPCs, but not Hdc-GFP^{lo} HSPCs, and decreased the myeloid/HSPC ratio in Hdc-GFP^{hi} HSPCs, whereas the H_2 antagonist (ICI 162,846) selectively decreased Hdc-GFP^{hi} HSPC quiescence (Figures 5H, 5I, and S5P).

Finally, the effect of exogenous histamine was reproduced by the addition of histamine-producing myeloid cells to the Hdc-GFP^{hi} HSPC culture system. Similarly, the frequency of G0/quiescence Hdc-GFP^{hi} HSPCs was increased, while the cell cycle status of Hdc-GFP^{lo} or *H*$_2$*R*$^{-/-}$ HSPCs was unchanged (Figures S5Q and S5R). Taken together, these data suggest

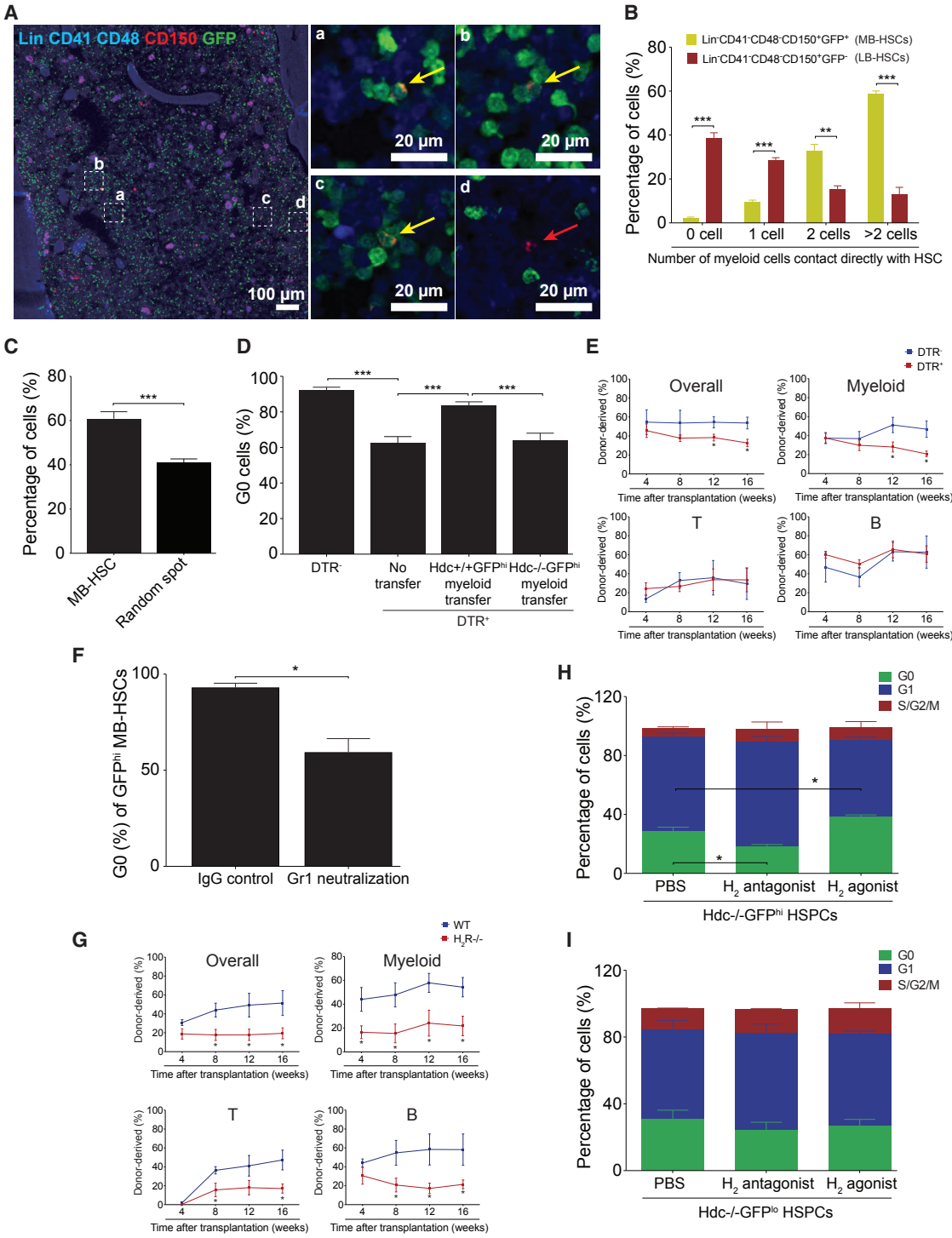

Figure 5. Histamine-Producing Myeloid Cells Maintain MB-HSCs

(A) Immunofluorescent images showing spatial relationship between MB-HSCs (A–C, yellow arrow, n = 198) or LB-HSCs (D, red arrow, n = 321) and Hdc-GFP^{+} myeloid cells.

(B) Quantitation of spatial relationships, showing number of myeloid cells in direct contact with HSCs.

(C) Percentages of MB-HSCs (n = 541) and random spots (n = 2,480) that contacted directly with ≥2 Hdc-GFP^{+} myeloid cells.

(D) G0 BM HSCs in Hdc-CreER^{T2}; tdTomato; iDTR (n = 6) and Hdc-CreER^{T2}; tdTomato mice (n = 6) as depicted in Figure S5E. Cell cycle rescue was performed by GFP^{hi}CD11b^{+}Gr1^{+} cell transfer (n = 8). *Hdc*$^{-/-}$; Hdc-GFP^{hi} myeloid cells were used as the control (n = 6).

(E) Percentage of donor-derived myeloid, T, and B cells in lethally irradiated recipients transplanted with unfractionated BM cells from Hdc-CreER^{T2}; tdTomato; iDTR or control mice (n = 5 per group).

(legend continued on next page)

that MB-HSCs and progenitors show (1) selective responses to histamine (2) in an H_2R-dependent manner and (3) that histamine-producing myeloid cells can enforce quiescence. The cluster of MB-HSCs and histamine-producing myeloid cells generates a histamine/H_2R axis with a *cis*-regulatory auto-/paracrine effect.

Histamine/H_2R Axis Protects MB-HSCs from Myelosuppressive Injury

Myelosuppressive injury leads to the disappearance of most myeloid cells, which triggers HSC proliferation and differentiation in order to rapidly replenish the BM myeloid pool. However, the price is often some degree of loss of self-renewal ability by HSCs. After irradiation (IR) injury to the hematopoietic system, we observed that the absolute number of HSCs and circulating myeloid cells decreased, along with a relative increase in the percentage of Hdc-GFP^{hi} HSCs and their BM myeloid descendants (Figures 6A, 6B, S6A, and S6B). The majority of Hdc-GFP^{hi} HSCs were quiescent at baseline (Figures 2F and 3C), and they exited dormancy shortly after IR (Figure S6C) to increase their myeloid colony-forming output (Figure S6D), suggesting that they fuel myeloid regeneration after myelotoxic injury.

In competitive transplantation assay, albeit with short-term follow-up (4–12 weeks), irradiated Hdc-GFP^{hi} HSPCs displayed higher donor cell reconstitution (in particular in myeloid lineage) compared to Hdc-GFP^{lo} controls. Thus, they might have lost the ability for LT myeloid reconstitution (Figure 6C).

Given that histamine can enforce MB-HSC quiescence, we wondered if *Hdc*$^{-/-}$ MB-HSCs might be disproportionately sensitive to IR injury. Gene profiling revealed a low expression of radiation resistance genes in *Hdc*$^{-/-}$ HSPCs (Figure S6E) (Table S1) (De Bacco et al., 2011; Grimbaldeston et al., 2003). *Hdc*$^{-/-}$ animals subjected to IR injury showed that BM Hdc-GFP^{hi} HSCs and myeloid cells were depleted dramatically and that *Hdc*$^{-/-}$;Hdc-GFP^{hi} myeloid cells recovered more slowly than WT controls at 10 days post-IR (Figures 6D, 6E, and S6F–S6I). However, H_2 agonist-treated *Hdc*$^{-/-}$ and WT mice both showed higher BM HSC numbers, while the protective effect of the H_2 agonist was abolished in *$H_2R^{-/-}$* mice (Figure S6J). Furthermore, the reconstitution capacity of Hdc-GFP^{hi} BM cells was significantly improved when donor mice received H_2 agonist 10 days prior to radiation (Figure 6F). Finally, H_2 agonist improved the overall survival of WT mice following lethal IR (Figure 6G). Taken together, these results suggest that exogenous H_2 agonist can protect MB-HSCs and progenitors from injury.

We next sought to determine whether histamine protects MB-HSCs and progenitors from LPS-induced stimulation and depletion. Consistent with previous observations (Rodriguez et al., 2009), LPS treatment promoted the activation of MB-HSCs and progenitors in the BM and increased splenic accumulation of myeloid progenitors, which was much more pronounced in *Hdc*$^{-/-}$ animals (Figures 6H and S6K). There was a considerable expansion of MB-MPPs (Hdc-GFP^{hi} MPP3) in *Hdc*$^{-/-}$ BM and spleen, whereas the frequencies of MB-HSCs and overall MPPs were decreased (Figures S6L and S6M), indicating an MB-HSC depletion phenotype. Treatment with the H_2 agonist in either LPS-treated *Hdc*$^{-/-}$ or WT mice significantly increased BM MB-HSC frequencies (Figure 6I).

DISCUSSION

Here we have identified a subset of MB-HSCs that express Hdc. Although largely quiescent, MB-HSCs and progenitors respond to myeloid stimulants with rapid expansion and production of Hdc^{hi} myeloid cells, but they are relatively resistant to IL-7. Within the BM, MB-HSCs are surrounded by Hdc^{hi} myeloid cells, which regulate the physiology of MB-HSCs through a histamine/H_2R axis. This feedback loop is important for maintaining MB-HSC dormancy under homeostatic conditions and preventing depletion in the setting of injury.

Our findings add to the growing evidence regarding the heterogeneity of HSCs and progenitors. Recent studies have cast some doubt on the stepwise hematopoiesis model (Notta et al., 2016; Yamamoto et al., 2013). Busch and coworkers further indicate that most of the hematopoietic lineages in the adult animal under homeostatic conditions are produced by large numbers of progenitors (e.g., Lin-Sca1 +Kit- hematopoietic cells [LSKs]), with LT-HSCs participating to a limited extent (Busch et al., 2015).

Acute injury requires a rapid and lineage-specific response, which thus demands an effective hierarchical organization of hematopoiesis. Previous studies proposed that sub-groups of HSCs and progenitors are dedicated to the generation of more limited classes of myeloid and platelet cells in both steady state and acute inflammation (Dutta et al., 2015). The Hdc-expressing HSCs demonstrated greater myeloid repopulation capacity, with more granulocyte clonogenic ability in transplantation and CFU assays (Figure 1). Hdc^{hi} HSCs showed higher levels of myeloid-specific genes but lower expression of lymphoid genes (Figure 1). Hdc^{hi} HSCs also exhibited much greater responsiveness to myeloid, but not lymphoid, stimulants, thus defining an MB-HSC population (Figures 2 and 3). These data further support the notion that, even within MB-HSCs, granulocytic and monocytic myeloid lineages can be distinguished at an early HSC stage.

MB-HSCs and progenitors respond quickly to leukopenia, triggered by LPS or direct myeloablative injury to BM (King and Goodell, 2011). Notably, such myeloid activation promoted Hdc^{hi} MB-HSCs and progenitors to enter the cell cycle, mobilized them into the circulation, and induced extramedullary hematopoiesis (Figure 2). Given the high expression of TLR4 on Hdc-GFP^{hi} HSCs and HSPCs and their increased number following LPS treatment (Figure 2), our results support a recent study that LPS can directly activate the proliferation of HSCs via TLR4 (Takizawa et al., 2017). Although LPS stimulation also can enhance the role of the histamine/H_2R axis through expansion of Hdc-GFP^{hi} myeloid cells to enforce the quiescence of MB-HSCs, the increased myeloid demand may over time overwhelm the inhibitory effects of the feedback loop, leading to

(F) G0 Hdc-GFP^{hi} MB-HSCs in Gr1 monoclonal antibody or rat IgG-treated mice (n = 3 per group).
(G) Donor chimerism in recipients transplanted with 2 × 10^5 WT or *$H_2R^{-/-}$* total BM cells along with the same number of CD45.1 BM cells (n = 10 per group).
(H and I) Hdc-GFP^{hi} HSPCs (H, n = 6) and Hdc-GFP^{lo} HSPCs (I, n = 5) co-cultured with *Hdc*$^{-/-}$ stromal cells and H_2 antagonist or agonist. Data were analyzed with Mann-Whitney test (B and C), one-way ANOVA with Bonferroni post hoc test (D, H, and I), or two-tailed Student's t test (E–G). See also Figure S5.

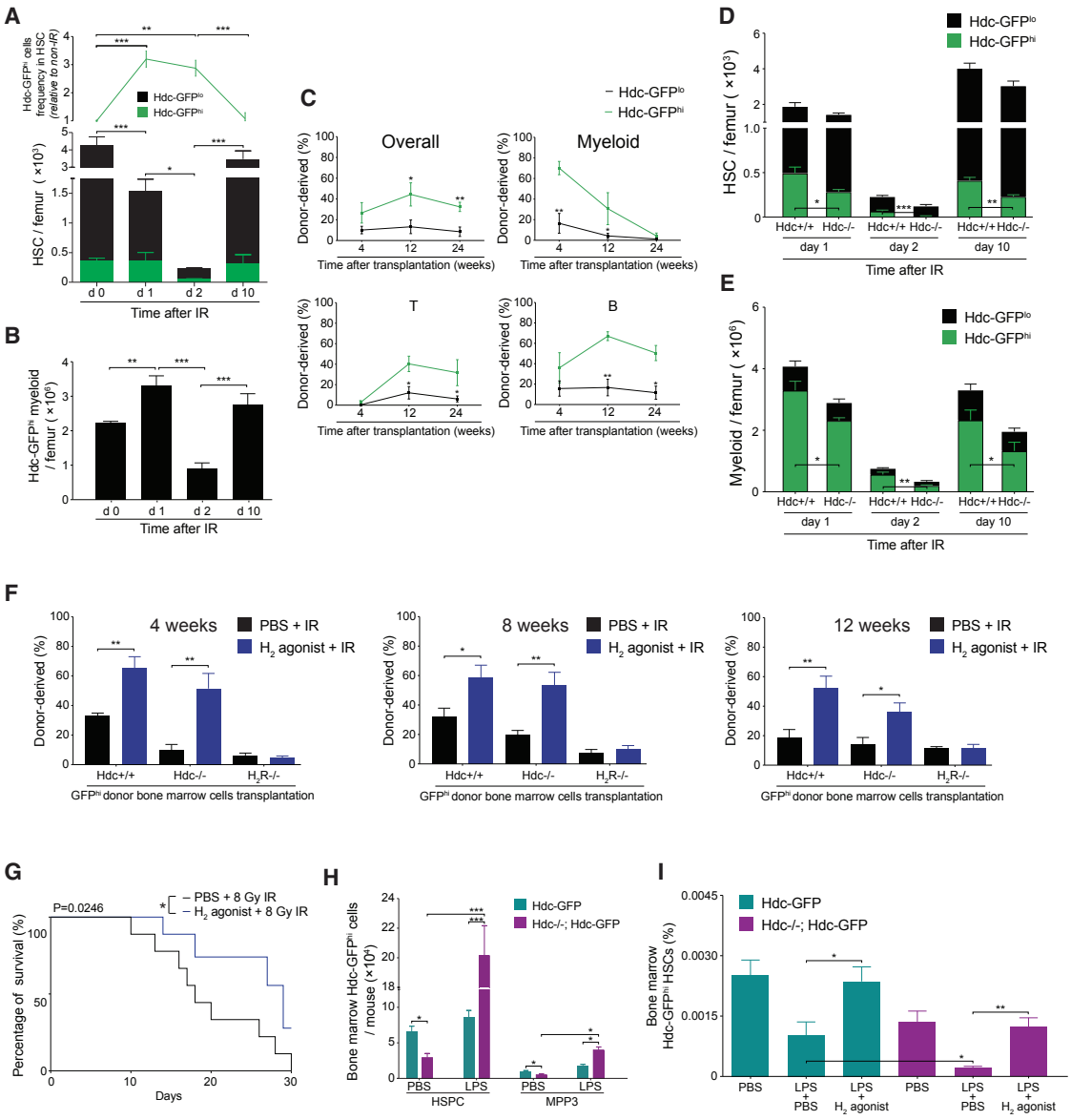

Figure 6. Myeloid-Derived Histamine Protects MB-HSCs from Myelosuppressive Injury

(A) Quantification of Hdc-GFP^{hi} HSCs in irradiated Hdc-GFP mice (n = 4–6 per time point).

(B) Number of BM Hdc-GFP^{+} myeloid cells in (A).

(C) Competitive reconstitution comparison between 3-Gy-irradiated 1,500 Hdc-GFP^{hi} and Hdc-GFP^{lo} HSPCs (n = 5 per group).

(D and E) Number of total HSCs (D) or myeloid cells (E) in 5-Gy-irradiated Hdc-GFP (n = 4) and *Hdc*$^{-/-}$; Hdc-GFP mice (n = 6).

(F) Blood chimerism of lethally irradiated recipients transplanted with 5 × 10^{5} unfractionated Hdc-GFP^{+} donor BM cells along with Sca-1-depleted CD45.1 BM cells (n = 5 each treatment).

(G) Survival of 8-Gy-irradiated mice pre-treated with either H_2 agonist or PBS (n = 15 per group).

(H) Absolute numbers of BM Hdc-GFP^{hi} HSPCs and MPP (MPP3) in LPS- or PBS-treated mice at 24 hr (n = 3–6 per group).

(I) Protective effect of H_2 agonist on LPS-induced sepsis mice (n = 5 per group). Data were analyzed with one-way ANOVA with Bonferroni post hoc test (A, B, and I), two-tailed Student's t test (C–F and H), or log rank test (G). See also Figure S6.

For all panels, ±SEM is shown (*p < 0.05, **p < 0.01, and ***p < 0.001; n.s., not significant; n.d., not detectable; n indicates biological replicates). For all experiments, greater than or equal to two independent experiments were performed unless otherwise indicated.

the depletion of Hdc-GFP^{hi} HSCs (Figure 2C). Further studies are required to confirm whether this belongs to the indirect effects of LPS on the behaviors of HSC (Takizawa et al., 2017).

MB-HSC is normally a quiescent LT-HSC, based on its slowly cycling nature and reconstitution ability (Challen et al., 2010; Land et al., 2015; Morita et al., 2010). Although it has previously been proposed that lineage-biased HSCs reside and communicate in distinct niches, few details have been reported (Yu and Scadden, 2016). Our anatomical studies revealed direct contacts between MB-HSC and Hdc^{hi} myeloid descendants.

Furthermore, we have shown that the quiescence and self-renewal of MB-HSCs were conferred by histamine in the niche (Figure 5). The MB-HSCs expressed a high level of H_2R, and the loss of histamine production in the niche as a result of either knockout of the Hdc gene or ablation of the Hdc^{hi} myeloid descendants led to increased proliferation of HSCs and progenitors, along with loss over time of MB-HSCs (Figure 4). The regulation of MB-HSC quiescence by myeloid lineage-derived histamine provides an elegant regulatory mechanism, such that the recruitment of myeloid cells out of BM by an infectious or injurious threat removes the inhibitory brake on MB-HSCs, thus awakening these stem cells from dormancy.

Given that histamine produced by Hdc^{hi} cells acted primarily through H_2R on MB-HSCs and progenitors, a selective H_2 agonist, dimaprit dihydrochloride, was effective *in vivo* or *in vitro* to rescue MB-HSC quiescence and improve their regenerative capacity (Figures 5 and 6). Treatment with the H_2 agonist prior to radiation injury protected MB-HSCs from depletion and significantly increased the lifespan and survival of lethally irradiated mice. Similarly, treatment with the exogenous H_2 agonist profoundly increased the numbers of $Hdc^{hi}H_2R^{+}$ stem cells and progenitors in LPS-induced sepsis and abrogated HSC depletion (Figure 6).

While the iDTR/DT ablation model has limitations, we found in this study that depletion of Hdc^{hi} myeloid cells had minimal effects on the Hdc^{lo} HSCs (Figures 5 and S5). Given the close spatial relationship between Hdc^{hi} myeloid cells and MB-HSCs and evidence that the histamine/H_2R axis regulates the quiescence of MB-HSCs, we reason that iDTR/DT ablation of Hdc^{hi} myeloid cells and subsequent loss of the majority of the histaminergic niche is the cause of MB-HSCs entering cell cycle. These findings favor the hypothesis that lineage-biased HSCs and progenitors are regulated in a lineage-dependent manner (Cordeiro Gomes et al., 2016).

Hdc^{hi} HSCs showed features consistent with previously identified MB-HSCs, such as $CD150^{hi}CD34^{-}KLS$ cells, HSC-1, lower-SP^{KLS} cells, $CD86^{-}$ HSCs, $CD41^{+}$ HSCs, and von Willebrand factor (vWF^{+}) HSCs (Challen et al., 2010; Gekas and Graf, 2013; Iida et al., 2014; Morita et al., 2010; Oguro et al., 2013; Sanjuan-Pla et al., 2013). First, our study supports earlier findings that suggested that MB-HSCs account for an extremely low number of total BM nucleated cells (around 0.002%). Second, consistent with the data regarding HSC-1 (Oguro et al., 2013), we found that Hdc^{hi} HSCs are more quiescent and can interconvert into other HSC subsets, but not vice versa. Third, we also found that aging led to an increase in the number of Hdc^{hi} HSCs, similar to results with lower-SP^{KLS} (Challen et al., 2010). Although some earlier studies reported that MB-HSCs accounted for a higher (5.67%–60%) proportion of HSCs, the Hdc^{hi} subset comprised only 10.3% ± 2.27% of all HSCs. However, $CD150^{hi}$HSCs contained myeloid- (HSC-1) and lymphoid-biased (HSC-2) subcategories (Oguro et al., 2013), whereas our study suggests that the Hdc^{hi} population represents a more myeloid-specific subset within the $CD150^{hi}$HSC pool. Further, in contrast to previous studies that primarily addressed surface markers and repopulation ability, we demonstrate here a clear role for the histamine/H_2R axis in maintaining homeostasis and quiescence of the MB-HSC pool.

In summary, Hdc labels a previously undefined but distinct MB-HSC that resides in the center of a cluster of mature Hdc-expressing myeloid cells. Homeostasis relies on a negative feedback histaminergic circuit, whereby histamine produced by Hdc-expressing cells inhibits active cycling in MB-HSCs through the H_2R in a lineage-privileged *cis*-regulatory auto-/paracrine fashion. The ablation of histamine-producing cells by genetic or other approaches leads to a loss of this inhibitory signal and exit from dormancy by the MB-HSCs. Mice deficient in histamine production ($Hdc^{-/-}$) or lacking the receptor ($H_2R^{-/-}$) showed exaggerated responses to myeloid demand hematopoiesis and reductions in the MB-HSC and progenitor pool. Histaminergic signaling through the H_2R on MB-HSC limits excessive proliferation and promotes self-renewal. Targeting the histamine/H_2R axis may thus be useful therapeutically in protecting MB-HSCs from myelosuppressive injury and stem cell depletion.

STAR★METHODS

Detailed methods are provided in the online version of this paper and include the following:

- KEY RESOURCES TABLE
- CONTACT FOR REAGENTS AND RESOURCE SHARING
- EXPERIMENTAL MODEL AND SUBJECT DETAILS
  - Mice
- METHOD DETAILS
  - Flow cytometry analysis and cell sorting
  - Bone marrow transplantation
  - Hematopoietic stem cells and progenitors colony-forming assay
  - *In vivo* treatments
  - Quantitative RT-PCR
  - RNA-seq analysis
  - Microarray gene expression profiling
  - Cell culture and protein detection
  - Immunofluorescence microscopy
  - Reproducibility
- QUANTIFICATION AND STATISTICAL ANALYSIS
  - Gene expression microarray analysis
  - Analysis of RNA-seq data
  - Computational modeling of HSC distribution
- DATA AND SOFTWARE AVAILABILITY

SUPPLEMENTAL INFORMATION

Supplemental Information includes six figures and one table and can be found with this article online at https://doi.org/10.1016/j.stem.2017.11.003.

AUTHOR CONTRIBUTIONS

X.C. and H. Deng conceptualized and designed the study, performed the experiments, interpreted the data, and wrote the manuscript. M.J.C., X.D., S.-H.H., S.V.S., P.T., Z.J., and F.B. contributed to flow cytometric analysis or cell cultures. T.H.C., T.C.S., and L.M. acquired and computationally analyzed fluorescence confocal images. R.A.F., H. Ding, A.L.E.W., and A.C. performed and analyzed RNA-seq and microarray experiments. L.L.L., M.M., and R.A.F. also participated in the manuscript writing. K.K.N., Y.H.T., H.L., Z.N., H.W., W.C., R.T., B.W.R., and Y.H. participated in mouse handling, irradiation, or bone marrow transplantation. S.R. provided expertise on the bone section and immunostaining. D.L.W., C.B.W., S.A., C.-S.L., and

H.-W.S. contributed to transgenic mouse constructor design or manuscript revision. T.C.W. and S.M. supervised the project, including study design, data interpretation, and manuscript writing.

ACKNOWLEDGMENTS

This work was supported by NIH NIDDK to T.C.W. (5R01DK048077) and NHLBI to S.M. (5R01HL115145). H. Deng was supported by the grant from the National Science Foundation of China (81770624). M.M. was supported by a postdoctoral fellowship grant from the Mildred-Scheel-Stiftung, Deutsche Krebshilfe, Germany (70111870). H.W. was supported by the Shanghai Pujiang Program of China (16PJ1401900). R.T. was supported by the Uehara Memorial Foundation. We thank Dr. Kazuhiko Yanai and Dr. Takeo Yoshikawa from Tohoku University School of Medicine, Japan, for providing $H_2R^{-/-}$ mice. We thank Dr. Caisheng Lu and Dr. Wei Wang from the CCTI Flow Cytometry Core (supported in part by the Office of the Director, NIH, under awards S10OD020056 and S10RR027050). Images were collected and analyzed at the Confocal and Specialized Microscopy Shared Resource of the Herbert Irving Comprehensive Cancer Center at Columbia University, supported by NIH grant P30 CA013696 (National Cancer Institute). We thank Dr. Xiangdong Yang, Ms. Sarah Stokes, and Ms. Ashlesha Muley for helping to generate the Hdc-CreER^{T2} construct. We gratefully acknowledge Dr. Lei Ding at Columbia University for the discussions and providing the Cryojane system for the preparation of mouse bone sections. We also thank Dr. Jianchun Chen at Columbia University for the discussions. Finally, we express our greatest appreciation and admiration for Dr. Xiaowei Chen, who devoted his postdoctoral career to this study and made most of the original observations reported here. Sadly, he passed away in April 2017, during the revision of the manuscript.

Received: April 18, 2017
Revised: August 4, 2017
Accepted: November 1, 2017
Published: November 30, 2017

REFERENCES

Alcañiz, L., Vega, A., Chacón, P., El Bekay, R., Ventura, I., Aroca, R., Blanca, M., Bergstralh, D.T., and Monteseirin, J. (2013). Histamine production by human neutrophils. FASEB J. *27*, 2902–2910.

Ardi, V.C., Kupriyanova, T.A., Deryugina, E.I., and Quigley, J.P. (2007). Human neutrophils uniquely release TIMP-free MMP-9 to provide a potent catalytic stimulator of angiogenesis. Proc. Natl. Acad. Sci. USA *104*, 20262–20267.

Beerman, I., Maloney, W.J., Weissmann, I.L., and Rossi, D.J. (2010). Stem cells and the aging hematopoietic system. Curr. Opin. Immunol. *22*, 500–506.

Benjamini, Y., and Hochberg, Y. (1995). Controlling the false discovery rate: a practical and powerful approach to multiple testing. J. R. Stat. Soc. Series B Methodol. *57*, 289–300.

Broxmeyer, H.E., Hoggatt, J., O'Leary, H.A., Mantel, C., Chitteti, B.R., Cooper, S., Messina-Graham, S., Hangoc, G., Farag, S., Rohrabaugh, S.L., et al. (2012). Dipeptidylpeptidase 4 negatively regulates colony-stimulating factor activity and stress hematopoiesis. Nat. Med. *18*, 1786–1796.

Brune, M., Castaigne, S., Catalano, J., Gehlsen, K., Ho, A.D., Hofmann, W.K., Hogge, D.E., Nilsson, B., Or, R., Romero, A.I., et al. (2006). Improved leukemia-free survival after postconsolidation immunotherapy with histamine dihydrochloride and interleukin-2 in acute myeloid leukemia: results of a randomized phase 3 trial. Blood *108*, 88–96.

Bruns, I., Lucas, D., Pinho, S., Ahmed, J., Lambert, M.P., Kunisaki, Y., Scheiermann, C., Schiff, L., Poncz, M., Bergman, A., and Frenette, P.S. (2014). Megakaryocytes regulate hematopoietic stem cell quiescence through CXCL4 secretion. Nat. Med. *20*, 1315–1320.

Busch, K., Klapproth, K., Barile, M., Flossdorf, M., Holland-Letz, T., Schlenner, S.M., Reth, M., Höfer, T., and Rodewald, H.R. (2015). Fundamental properties of unperturbed haematopoiesis from stem cells in vivo. Nature *518*, 542–546.

Challen, G.A., Boles, N.C., Chambers, S.M., and Goodell, M.A. (2010). Distinct hematopoietic stem cell subtypes are differentially regulated by TGF-beta1. Cell Stem Cell *6*, 265–278.

Chen, X., Takemoto, Y., Deng, H., Middelhoff, M., Friedman, R.A., Chu, T.H., Churchill, M.J., Ma, Y., Nagar, K.K., Tailor, Y.H., et al. (2017). Histidine decarboxylase (HDC)-expressing granulocytic myeloid cells induce and recruit Foxp3(+) regulatory T cells in murine colon cancer. OncoImmunology *6*, e1290034.

Cheung, T.H., and Rando, T.A. (2013). Molecular regulation of stem cell quiescence. Nat. Rev. Mol. Cell Biol. *14*, 329–340.

Cordeiro Gomes, A., Hara, T., Lim, V.Y., Herndler-Brandstetter, D., Nevius, E., Sugiyama, T., Tani-Ichi, S., Schlenner, S., Richie, E., Rodewald, H.R., et al. (2016). Hematopoietic Stem Cell Niches Produce Lineage-Instructive Signals to Control Multipotent Progenitor Differentiation. Immunity *45*, 1219–1231.

De Bacco, F., Luraghi, P., Medico, E., Reato, G., Girolami, F., Perera, T., Gabriele, P., Comoglio, P.M., and Boccaccio, C. (2011). Induction of MET by ionizing radiation and its role in radioresistance and invasive growth of cancer. J. Natl. Cancer Inst. *103*, 645–661.

de Bruin, A.M., Libregts, S.F., Valkhof, M., Boon, L., Touw, I.P., and Nolte, M.A. (2012). IFNγ induces monopoiesis and inhibits neutrophil development during inflammation. Blood *119*, 1543–1554.

Dias, S., Silva, H., Jr., Cumano, A., and Vieira, P. (2005). Interleukin-7 is necessary to maintain the B cell potential in common lymphoid progenitors. J. Exp. Med. *201*, 971–979.

Ding, L., and Morrison, S.J. (2013). Haematopoietic stem cells and early lymphoid progenitors occupy distinct bone marrow niches. Nature *495*, 231–235.

Dutta, P., Sager, H.B., Stengel, K.R., Naxerova, K., Courties, G., Saez, B., Silberstein, L., Heidt, T., Sebas, M., Sun, Y., et al. (2015). Myocardial Infarction Activates CCR2(+) Hematopoietic Stem and Progenitor Cells. Cell Stem Cell *16*, 477–487.

Gekas, C., and Graf, T. (2013). CD41 expression marks myeloid-biased adult hematopoietic stem cells and increases with age. Blood *121*, 4463–4472.

Grimbaldeston, M.A., Geczy, C.L., Tedla, N., Finlay-Jones, J.J., and Hart, P.H. (2003). S100A8 induction in keratinocytes by ultraviolet A irradiation is dependent on reactive oxygen intermediates. J. Invest. Dermatol. *121*, 1168–1174.

Guo, F., Velu, C.S., Grimes, H.L., and Zheng, Y. (2009). Rho GTPase Cdc42 is essential for B-lymphocyte development and activation. Blood *114*, 2909–2916.

Hart, G.W., Slawson, C., Ramirez-Correa, G., and Lagerlof, O. (2011). Cross talk between O-GlcNAcylation and phosphorylation: roles in signaling, transcription, and chronic disease. Annu. Rev. Biochem. *80*, 825–858.

Hu, Y., and Smyth, G.K. (2009). ELDA: extreme limiting dilution analysis for comparing depleted and enriched populations in stem cell and other assays. J. Immunol. Methods *347*, 70–78.

Iida, R., Welner, R.S., Zhao, W., Alberola-Ila, J., Medina, K.L., Zhao, Z.J., and Kincade, P.W. (2014). Stem and progenitor cell subsets are affected by JAK2 signaling and can be monitored by flow cytometry. PLoS ONE *9*, e93643.

Jung, J., Bohn, G., Allroth, A., Boztug, K., Brandes, G., Sandrock, I., Schäffer, A.A., Rathinam, C., Köllner, I., Beger, C., et al. (2006). Identification of a homozygous deletion in the AP3B1 gene causing Hermansky-Pudlak syndrome, type 2. Blood *108*, 362–369.

King, K.Y., and Goodell, M.A. (2011). Inflammatory modulation of HSCs: viewing the HSC as a foundation for the immune response. Nat. Rev. Immunol. *11*, 685–692.

Klimenkova, O., Ellerbeck, W., Klimiankou, M., Ünalan, M., Kandabarau, S., Gigina, A., Hussein, K., Zeidler, C., Welte, K., and Skokowa, J. (2014). A lack of secretory leukocyte protease inhibitor (SLPI) causes defects in granulocytic differentiation. Blood *123*, 1239–1249.

Land, R.H., Rayne, A.K., Vanderbeck, A.N., Barlowe, T.S., Manjunath, S., Gross, M., Eiger, S., Klein, P.S., Cunningham, N.R., Huang, J., et al. (2015). The orphan nuclear receptor NR4A1 specifies a distinct subpopulation of quiescent myeloid-biased long-term HSCs. Stem Cells *33*, 278–288.

Matatall, K.A., Jeong, M., Chen, S., Sun, D., Chen, F., Mo, Q., Kimmel, M., and King, K.Y. (2016). Chronic Infection Depletes Hematopoietic Stem Cells through Stress-Induced Terminal Differentiation. Cell Rep. *17*, 2584–2595.

Morita, Y., Ema, H., and Nakauchi, H. (2010). Heterogeneity and hierarchy within the most primitive hematopoietic stem cell compartment. J. Exp. Med. *207*, 1173–1182.

Morrison, S.J., and Scadden, D.T. (2014). The bone marrow niche for haematopoietic stem cells. Nature *505*, 327–334.

Nagai, Y., Garrett, K.P., Ohta, S., Bahrun, U., Kouro, T., Akira, S., Takatsu, K., and Kincade, P.W. (2006). Toll-like receptors on hematopoietic progenitor cells stimulate innate immune system replenishment. Immunity *24*, 801–812.

Notta, F., Zandi, S., Takayama, N., Dobson, S., Gan, O.I., Wilson, G., Kaufmann, K.B., McLeod, J., Laurenti, E., Dunant, C.F., et al. (2016). Distinct routes of lineage development reshape the human blood hierarchy across ontogeny. Science *351*, aab2116.

Oguro, H., Ding, L., and Morrison, S.J. (2013). SLAM family markers resolve functionally distinct subpopulations of hematopoietic stem cells and multipotent progenitors. Cell Stem Cell *13*, 102–116.

Rodriguez, S., Chora, A., Goumnerov, B., Mumaw, C., Goebel, W.S., Fernandez, L., Baydoun, H., HogenEsch, H., Dombkowski, D.M., Karlewicz, C.A., et al. (2009). Dysfunctional expansion of hematopoietic stem cells and block of myeloid differentiation in lethal sepsis. Blood *114*, 4064–4076.

Saligrama, N., Noubade, R., Case, L.K., del Rio, R., and Teuscher, C. (2012). Combinatorial roles for histamine H1-H2 and H3-H4 receptors in autoimmune inflammatory disease of the central nervous system. Eur. J. Immunol. *42*, 1536–1546.

Sanjuan-Pla, A., Macaulay, I.C., Jensen, C.T., Woll, P.S., Luis, T.C., Mead, A., Moore, S., Carella, C., Matsuoka, S., Bouriez Jones, T., et al. (2013). Platelet-biased stem cells reside at the apex of the haematopoietic stem-cell hierarchy. Nature *502*, 232–236.

Schinke, C., Giricz, O., Li, W., Shastri, A., Gordon, S., Barreyro, L., Bhagat, T., Bhattacharyya, S., Ramachandra, N., Bartenstein, M., et al. (2015). IL8-CXCR2 pathway inhibition as a therapeutic strategy against MDS and AML stem cells. Blood *125*, 3144–3152.

Schürch, C.M., Riether, C., and Ochsenbein, A.F. (2014). Cytotoxic CD8+ T cells stimulate hematopoietic progenitors by promoting cytokine release from bone marrow mesenchymal stromal cells. Cell Stem Cell *14*, 460–472.

Shi, X., Siggins, R.W., Stanford, W.L., Melvan, J.N., Basson, M.D., and Zhang, P. (2013). Toll-like receptor 4/stem cell antigen 1 signaling promotes hematopoietic precursor cell commitment to granulocyte development during the granulopoietic response to Escherichia coli bacteremia. Infect. Immun. *81*, 2197–2205.

Siggs, O.M., Arnold, C.N., Huber, C., Pirie, E., Xia, Y., Lin, P., Nemazee, D., and Beutler, B. (2011). The P4-type ATPase ATP11C is essential for B lymphopoiesis in adult bone marrow. Nat. Immunol. *12*, 434–440.

Takeuchi, O., Hoshino, K., Kawai, T., Sanjo, H., Takada, H., Ogawa, T., Takeda, K., and Akira, S. (1999). Differential roles of TLR2 and TLR4 in recognition of gram-negative and gram-positive bacterial cell wall components. Immunity *11*, 443–451.

Takizawa, H., Fritsch, K., Kovtonyuk, L.V., Saito, Y., Yakkala, C., Jacobs, K., Ahuja, A.K., Lopes, M., Hausmann, A., Hardt, W.D., et al. (2017). Pathogen-Induced TLR4-TRIF Innate Immune Signaling in Hematopoietic Stem Cells Promotes Proliferation but Reduces Competitive Fitness. Cell Stem Cell *21*, 225–240.e5.

Terskikh, A.V., Miyamoto, T., Chang, C., Diatchenko, L., and Weissman, I.L. (2003). Gene expression analysis of purified hematopoietic stem cells and committed progenitors. Blood *102*, 94–101.

Trumpp, A., Essers, M., and Wilson, A. (2010). Awakening dormant haematopoietic stem cells. Nat. Rev. Immunol. *10*, 201–209.

Viatour, P., Somervaille, T.C., Venkatasubrahmanyam, S., Kogan, S., McLaughlin, M.E., Weissman, I.L., Butte, A.J., Passegué, E., and Sage, J. (2008). Hematopoietic stem cell quiescence is maintained by compound contributions of the retinoblastoma gene family. Cell Stem Cell *3*, 416–428.

Yamamoto, R., Morita, Y., Ooehara, J., Hamanaka, S., Onodera, M., Rudolph, K.L., Ema, H., and Nakauchi, H. (2013). Clonal analysis unveils self-renewing lineage-restricted progenitors generated directly from hematopoietic stem cells. Cell *154*, 1112–1126.

Yang, X.D., Ai, W., Asfaha, S., Bhagat, G., Friedman, R.A., Jin, G., Park, H., Shykind, B., Diacovo, T.G., Falus, A., and Wang, T.C. (2011). Histamine deficiency promotes inflammation-associated carcinogenesis through reduced myeloid maturation and accumulation of CD11b+Ly6G+ immature myeloid cells. Nat. Med. *17*, 87–95.

Yu, V.W., and Scadden, D.T. (2016). Heterogeneity of the bone marrow niche. Curr. Opin. Hematol. *23*, 331–338.

Zhao, M., Perry, J.M., Marshall, H., Venkatraman, A., Qian, P., He, X.C., Ahamed, J., and Li, L. (2014). Megakaryocytes maintain homeostatic quiescence and promote post-injury regeneration of hematopoietic stem cells. Nat. Med. *20*, 1321–1326.

STAR★METHODS

KEY RESOURCES TABLE

REAGENT or RESOURCE	SOURCE	IDENTIFIER
Antibodies		
Biotin anti-mouse CD2	BioLegend	Cat#: 100103 RRID: AB_312650
PerCP/Cy5.5 anti-mouse CD2	BioLegend	Cat#: 100115 RRID: AB_2563501
Biotin anti-mouse CD3	BioLegend	Cat#: 100243 RRID: AB_2563946
PerCP/Cy5.5 anti-mouse CD3	BioLegend	Cat#: 100217 RRID: AB_1595597
APC anti-mouse CD3	BioLegend	Cat#: 100235 RRID: AB_2561455
PE/Cy7 anti-mouse CD3	BioLegend	Cat#: 100219 RRID: AB_1732068
Biotin anti-mouse CD5	BioLegend	Cat#: 100603 RRID: AB_312732
PerCP/Cy5.5 anti-mouse CD5	BioLegend	Cat#: 100623 RRID: AB_2563432
Biotin anti-mouse CD8a	BioLegend	Cat#: 100703 RRID: AB_312742
PerCP/Cy5.5 anti-mouse CD8a	BioLegend	Cat#: 100733 RRID: AB_2075239
Biotin anti-mouse TER-119	BioLegend	Cat#: 116203 RRID: AB_313704
PerCP/Cy5.5 anti-mouse TER-119	BioLegend	Cat#: 116227 RRID: AB_893638
APC anti-mouse TER119	BioLegend	Cat#: 116211 RRID: AB_313712
Biotin anti-mouse Ly-6G/Ly-6C (Gr-1)	BioLegend	Cat#: 108403 RRID: AB_313368
PerCP/Cy5.5 anti-mouse Ly-6G/Ly-6C (Gr-1)	BioLegend	Cat#: 108427 RRID: AB_893561
APC/Cy7 anti-mouse Ly-6G/Ly-6C (Gr-1)	BioLegend	Cat#: 108423 RRID: AB_2137486
Brilliant Violet 421 anti-mouse Ly-6G/Ly-6C (Gr-1)	BioLegend	Cat#: 108433 RRID: AB_10900232
Purified anti-mouse Ly-6G/Ly-6C (Gr-1)	BioLegend	Cat# 108401 RRID: AB_313366
Biotin anti-mouse/human CD45R/B220	BioLegend	Cat#: 103203 RRID: AB_312988
APC/Cy7 anti-mouse/human CD45R/B220	BioLegend	Cat#: 103223 RRID: AB_313006
PerCP/Cy5.5 anti-mouse/human CD45R/B220	BioLegend	Cat#: 103235 RRID: AB_893356
Biotin anti-mouse CD41	BioLegend	Cat#: 133930 RRID: AB_2572133
APC anti-mouse CD41	BioLegend	Cat#: 133913 RRID: AB_11126751
APC anti-mouse CD31	BioLegend	Cat#: 102409 RRID: AB_312904
Biotin anti-mouse CD48	BioLegend	Cat#: 103409 RRID: AB_528826
APC anti-mouse CD48	BioLegend	Cat#: 103411 RRID: AB_571996
Biotin anti-mouse CD127 (IL-7Rα)	BioLegend	Cat#: 135005 RRID: AB_1953262
PE anti-mouse CD127 (IL-7Rα)	BioLegend	Cat#: 135009 RRID: AB_1937252
PerCP/Cy5.5 anti-mouse CD127 (IL-7Rα)	BioLegend	Cat#: 135021 RRID: AB_1937274
APC/Cy7 anti-mouse CD117 (c-kit)	BioLegend	Cat#: 105825 RRID: AB_1626280
PE/Cy7 anti-mouse Ly-6A/E (Sca-1)	BioLegend	Cat#: 122513 RRID: AB_756198
PE anti-mouse CD150 (SLAM)	BioLegend	Cat#: 115903 RRID: AB_313682
Brilliant Violet 785 anti-mouse CD150 (SLAM)	BioLegend	Cat#: 115937 RRID: AB_2565962
Anti-Mouse CD34 eFluor 660	eBioscience	Cat#: 50-0341-80 RRID: AB_10609352
PE anti-mouse CD16/32	BioLegend	Cat#: 101307 RRID: AB_312806
PE anti-mouse CD135	BioLegend	Cat#: 135305 RRID: AB_1877218
APC anti-mouse CD135	BioLegend	Cat#: 135309 RRID: AB_1953264
PE anti-mouse CD201 (EPCR)	BioLegend	Cat#: 141503 RRID: AB_10899579
APC anti-mouse CD201 (EPCR)	BioLegend	Cat#: 141505 RRID: AB_2561361
PE/Cy7 anti-mouse CX3CR1	BioLegend	Cat#: 149015 RRID: AB_2565699
PE anti-mouse CD115	BioLegend	Cat#: 135505 RRID: AB_1937254
APC anti-mouse/human CD11b	BioLegend	Cat#: 101211 RRID: AB_312794
PerCP/Cy5.5 anti-mouse CD45.1	BioLegend	Cat#: 110727 RRID: AB_893348
Brilliant Violet 785 anti-mouse CD45.1	BioLegend	Cat#: 110743 RRID: AB_2563379

(*Continued on next page*)

Continued

REAGENT or RESOURCE	SOURCE	IDENTIFIER
Pacific Blue anti-mouse CD45.2	BioLegend	Cat#: 109819 RRID: AB_492873
PE anti-mouse CD45.2	BioLegend	Cat#: 109807 RRID: AB_313444
PE anti-mouse CD45	BioLegend	Cat#: 103105 RRID: AB_312970
APC anti-mouse CD45	BioLegend	Cat#: 103111 RRID: AB_312976
PE anti-BrdU Antibody	BioLegend	Cat#: 339811 RRID: AB_1626188
PE anti-mouse Ki-67	BioLegend	Cat#: 652403 RRID: AB_2561524
Anti-Ki67 antibody	Abcam	Cat#: ab16667 RRID: AB_302459
Anti-GFP antibody	Abcam	Cat#: ab13970 RRID: AB_300798
RFP Antibody Pre-adsorbed	Rockland Immunochemicals	Cat#: 600-401-379 RRID: AB_2209751
Anti-Laminin 1+2 antibody	Abcam	Cat#: ab7463 RRID: AB_305933
Goat anti-Chicken, Alexa Fluor 488	Thermo Fisher Scientific	Cat# A-11039
Alexa Fluor 405 Streptavidin	Thermo Fisher Scientific	Cat# S32351
Goat anti-Rabbit IgG, Alexa Fluor 594	Thermo Fisher Scientific	Cat# R37117
Chemicals, Peptides, and Recombinant Proteins		
HBSS - Hank's Balanced Salt Solution	GIBCO	14175079
DPBS, no calcium, no magnesium	GIBCO	14190250
Minimum Essential Medium (MEM) Alpha Medium	Corning	10-022-CV
Fetal Bovine Serum	GIBCO	16140071
RBC Lysis Buffer (10X)	BioLegend	420301
Collagenase, Type 4	Worthington Biochemical Corporation	LS004186
DNase I	Roche Diagnostics	3724778103
BD Horizon BrilliantTM Stain Buffer	BD Biosciences	563794
Recombinant Mouse SCF (carrier-free)	BioLegend	579702
Recombinant Mouse Thrombopoietin (TPO)	BioLegend	593302
Recombinant Mouse GM-CSF	BioLegend	576302
Recombinant Mouse IL-6	BioLegend	575702
Recombinant Mouse IL-7	BioLegend	577802
Recombinant Mouse IFN-γ	BioLegend	575302
ProLong® Gold Antifade Mountant	Thermo Fisher Scientific	P36934
DAPI Solution	BD PharMingen	564907
Hoechst 33342 Solution	BD PharMingen	561908
LPS-EB Ultrapure	InvivoGen	tlrl-3pelps
Histamine dihydrochloride	Tocris Bioscience	3545
Dimaprit dihydrochloride	Tocris Bioscience	506
ICI 162,846	Tocris Bioscience	833
5-Fluorouracil	Sigma-Aldrich	3738
TAM Diet	Envigo Teklad Diets	TD.130859
Diphtheria Toxin	List Biological Labs	150
Percoll	GE Healthcare	17-0891-01
Critical Commercial Assays		
BrdU Flow Kits	BD PharMingen	552598
Histamine ELISA kit	Enzo Life Sciences	ENZ-KIT140-0001
IL6 ELISA kit	Thermo Fisher Scientific	KMC0061
IL7 ELISA kit	Thermo Fisher Scientific	EMIL7
IFN-γ ELISA kit	Thermo Fisher Scientific	88-8314-22
SMARTer Ultra Low Input RNA Kit for Sequencing	Clontech Laboratories	634849
Nextera XT DNA Library Preparation Kit	Illumina	FC-131-1024
CD117 MicroBeads	Miltenyi Biotec	130-091-224

(*Continued on next page*)

Continued

REAGENT or RESOURCE	SOURCE	IDENTIFIER
MidiMACS Separator and Starting Kits	Miltenyi Biotec	130-042-301
RNeasy Micro Kit	QIAGEN	74004
ARCTURUS PicoPure RNA Isolation Kit	Thermo Fisher Scientific	KIT0204
SuperScript III First-Strand Synthesis System	Thermo Fisher Scientific	18080051
PrimeTime qPCR Assays	Integrated DNA Technologies	N/A
FastStart Universal SYBR Green Master (Rox)	Roche Molecular Systems	4913850001
GeneChip Mouse Genome 430 2.0 Array	Thermo Fisher Scientific	900497
CryoJane Tape-Transfer system	Leica Biosystems	N/A
MethoCult GF M3434	STEMCELL Technologies	3444
MethoCult GF M3534	STEMCELL Technologies	3534
MethoCult M3630	STEMCELL Technologies	3630
Deposited Data		
GEO: Gene expression comparison between bone marrow Hdc-GFP^{hi}CD11b^{+}Gr1^{+} and Hdc-GFP^{lo}CD11b^{+}Gr1^{+}	N/A	GEO: GSE79728
GEO: Gene expression comparison between bone marrow Hdc-GFP^{hi}CD11b^{+}Gr1^{hi} and Hdc-GFP^{hi}CD11b^{+}Gr1^{lo}	N/A	GEO: GSE80143
GEO: Gene expression comparison between bone marrow Hdc-GFP^{hi} HSCs and Hdc-GFP^{lo} HSCs	N/A	GEO: GSE90787
GEO: Gene expression comparison between bone marrow Hdc-GFP^{hi} HSPCs and Hdc-GFP^{lo} HSPCs	N/A	GEO: GSE80092
GEO: Gene expression comparison between bone marrow *Hdc*$^{-/-}$ HSPCs and WT HSPCs	N/A	GEO: GSE80284
Experimental Models: Organisms/Strains		
Mouse: C57BL/6J	The Jackson Laboratory	Stock No: 000664
Mouse: B6.SJL-Ptprca Pepcb/BoyJ	The Jackson Laboratory	Stock No: 002014
Mouse: Gt(ROSA)26Sortm9(CAG-tdTomato)Hze/J	The Jackson Laboratory	Stock No: 007909
Mouse: C57BL/6-Gt(ROSA)26Sortm1(HBEGF)Awai/J	The Jackson Laboratory	Stock No: 007900
Mouse: Hdc-CreER^{T2}	This paper	N/A
Software and Algorithms		
ELDA: Extreme Limiting Dilution Analysis	Hu and Smyth, 2009	http://bioinf.wehi.edu.au/software/elda/
ImageJ version1.51h	N/A	http://imagej.net
Fiji version 2.0.0-rc54	N/A	http://imagej.net
Random_spots_noROI.py	This paper	https://github.com/theresaswayne/random-cells
FlowJo	FlowJo	https://www.flowjo.com
GraphPad Software	GraphPad Software	https://www.graphpad.com

CONTACT FOR REAGENTS AND RESOURCE SHARING

Further information and requests for resources and reagents should be directed to and will be fulfilled by the Lead Contact, Timothy C. Wang (tcw21@columbia.edu).

EXPERIMENTAL MODEL AND SUBJECT DETAILS

Mice

C57BL/6 background Hdc-GFP, *Hdc*$^{-/-}$ and *H*$_2$*R*$^{-/-}$ mice have been described previously (Yang et al., 2011). Hdc-GFP was crossed to *Hdc*$^{-/-}$ or *H*$_2$*R*$^{-/-}$ to generate *Hdc*$^{-/-}$; Hdc-GFP or *H*$_2$*R*$^{-/-}$; Hdc-GFP mice, respectively. In these transgenic mouse lines, the Hdc or H_2R gene was inactivated by neomycin replacement, and the Hdc-GFP transgenic reporter indicates Hdc-expressing cells. In some experiments, Hdc-GFP was crossed to Cxcl12-DsRed mice to generate Hdc-GFP; Cxcl12-DsRed mice (Ding and Morrison, 2013). The Hdc-CreER^{T2} transgenic line was generated by using bacterial artificial chromosome (BAC) recombineering from clone

RP23-474H6. Founders were backcrossed to C57BL/6 mice for at least six generations. Hdc-CreER^{T2} was mated to Rosa26-CAG-loxp-stop-loxp-tdTomato (tdTomato) and Rosa26-loxp-stop-loxp-iDTR (iDTR) mice for generating Hdc-CreER^{T2}; tdTomato and Hdc-CreER^{T2}; tdTomato; iDTR mice. C57BL/6 WT mice and C57BL/6-SJL (CD45.1) bone marrow transplantation recipient mice were purchased from the Jackson Laboratory. Both male and female mice were used in all studies. In order to minimize aging-related myeloid-biased effects, young (4-month-old) transgenic miceand their littermates were used in the majority of experiments. 16-month-old Hdc-GFP and C57BL/6 WT mice were used to evaluate the effect of aging on the number of hematopoietic lineage cells.

Mice were observed carefully by laboratory staff and veterinarian personnel for health and activity. Mice were monitored to ensure that food and fluid intake meets their nutritional needs. Body weights were recorded at minimum weekly, and more often for animals requiring greater attention. Mice were maintained on wood chip bedding, and given *ad libitum* access to water and standard mouse chow, with 12-hour light/dark phase cycles. The colonies were specific pathogen free (SPF) and tested quarterly for known pathogens. Mice in the barrier facilities are housed in cages with microisolator tops on ventilated or static racks. All caging materials and bedding are autoclaved. Food is irradiated and water is either RO, autoclaved or acidified, depending on the barrier. All manipulations are performed in laminar flow hoods. Once animals are removed from a barrier, they are not returned. All personnel wear shoe covers, gloves, hair bonnets and gowns. All mouse studies were approved by the Columbia University Institutional Animal Care and Use Committee.

METHOD DETAILS

Flow cytometry analysis and cell sorting

Mouse bones were flushed or crushed using mortar and pestle with Ca^{2+} and Mg^{2+} free HBSS supplemented 2% heat-inactivated fetal bovine serum. For hematopoietic stem cells and progenitors sorting, bone marrow mononuclear cells were first purified by 40:80 Percoll gradient centrifugation followed by CD117 MicroBeads enrichment (Miltenyi Biotec). The enriched progenitor cells were sorted twice based on the HSC or HSPC surface markers. The experiments only proceeded if the final purity was > 96% as demonstrated during re-sorting (Figure S1A). Single cell suspension from spleen was obtained by mashing the tissue by a syringe plunger end against a cell strainer. Blood was collected in EDTA-containing Tubes (BD Diagnostics) through the puncture of submandibular vein. Red blood cells were lysed (RBC lysis buffer, BioLegend) before passing through a 70 μm nylon mesh. Hematopoietic stem and progenitor cells, BM stromal endothelial cells, mesenchymal progenitor cells, and BM stromal endothelial cells were defined by immunophenotype. HSPC: Lin$^-$c-kit$^+$Sca-1$^+$, LSK; HSC: LSKCD150$^+$CD48$^-$; CMP: Lin$^-$IL-7Ra$^-$c-kit$^+$Sca-1$^-$CD34$^+$CD16/32^{lo}; GMP: Lin$^-$IL-7Ra$^-$c-kit$^+$Sca-1$^-$CD34$^+$CD16/32^{hi}; MEP: Lin$^-$IL-7Ra$^-$c-kit$^+$Sca-1$^-$CD34$^-$CD16/32^{lo}; MDP: Lin$^-$Flt-3$^+$c-kit^{hi}CD115$^+$CX3CR1$^+$; CDP: Lin$^-$Flt-3$^+$c-kit^{lo}CD115$^+$Cx3cr1$^+$; CLP: Lin$^-$c-kit^{lo}Sca-1^{lo}Flt-3$^+$IL-7Ra$^+$; myeloid cell: CD11b$^+$Gr1$^+$; bone marrow stromal endothelial cells (CD45$^-$Ter119$^-$CD31$^+$) and mesenchymal progenitor cells (CD45$^-$Ter119$^-$CD31$^-$). In IFN-γ-related experiments, Sca-1 was excluded from the stem and lineage-specific progenitor cell staining scheme because of its non-specific expression. The combination of LKCD150$^+$CD48$^-$CD34$^-$Flt-3$^-$EPCR$^+$ was used to define HSC (Matatall et al., 2016). Following antibodies were used: CD150 (TC15-12F12.2), CD48 (HM48-1), c-kit (2B8), Sca-1 (E13-161.7), CD34 (RAM34), CD16/32 (FcγR, 93), CD127 (IL7Ra, A7R34), CD135 (Flt-3, A2F10), CD115 (CSF-1R, AFS98), CD201 (EPCR, RCR-16), and CX3CR1 (SA011F11). Lineage cells were stained by using CD2 (RM2-5), CD3 (17A2), CD5 (53-7.3), CD8a (53-6.7), TER-119 (TER-119), B220 (RA3-6B2), and Gr1 (RB6-8C5). Other antibodies used in this study include CD41 (MEReg30), CD31 (MEC 13.3), CD11b (M1/70), CD45 (30-F11), CD45.1 (A20) and CD45.2 (104). For mouse bone stroma flow analysis, collagenase IV (Worthington Biochemical Corporation) and DNase I (Roche Diagnostics) were used to digest the marrow flushed long bones (Ding and Morrison, 2013). Supernatants from enzymatically digested mouse bones were filtered, washed and antibody-stained. DAPI (4',6-Diamidino-2-Phenylindole, Dihydrochloride) was used to exclude dead cells. For cell cycle analysis, sorted GFP^{hi} or GFP^{lo} cells were first stained with cell surface markers, then fixed and permeablized (BD cytofix/cytoperm solutions), followed by staining with anti-Ki67 (16A8) and Hoechst 33342 (BD PharMingen). For BrdU incorporation experiments, Hdc-GFP^{hi} and Hdc-GFP^{lo} cells were separated and analyzed by using BD PharMingen™ BrdU Flow Kits, according to manufacturer's instructions. All FACS analyses were performed on LSRII or LSRFortessa instrument. BD Influx cell sorter was used for cell sorting.

Bone marrow transplantation

Recipient CD45.1 mice were lethally irradiated (11 Gy, two split doses, at least 6 hours apart) using a Cesium 137 irradiator (Mark I-30, JL Shepherd and Associates). Sorted HSCs, HSPCs, or unfractionated bone marrow cells were injected intravenously along with CD45.1 competitor bone marrow cells. For single HSC transplantation, single Hdc-GFP^{hi} or Hdc-GFP^{lo} HSCs from bone marrow of Hdc-GFP mice were sorted directly into X-VIVO™ 15 medium (supplemented with 50 ng/ml of SCF and TPO). Single HSC was confirmed visually by using a microscope and then were transferred along with 2 × 10^5 CD45.1 whole bone marrow cells into lethally irradiated recipients. Flow analysis 16 to 32 weeks post transplantation of recipient blood showing ≥ 0.1% CD45.2 donor contribution is defined as the successful reconstitution. To compare the reconstitution capacity of Hdc-GFP^{hi} and Hdc-GFP^{lo} HSPCs affected by irradiation, 1500 sorted donor Hdc-GFP^{hi} or Hdc-GFP^{lo} HSPCs were 3 Gy irradiated and then transplanted along with 2 × 10^5 whole recipient bone marrow cells. In some experiments, donor mice were pretreated with either PBS or H_2 agonist and irradiated (3 Gy) before bone marrow Hdc-GFP^{hi} cells were harvested and transplanted with the same numbers of Sca-1-depleted recipient bone marrow cells. Recipient mice were bled between 4 to 8 weeks intervals starting from the fourth week after transplantation.

Multiple-lineage cells were assessed by flow analysis. Secondary bone marrow transplantation was performed by injecting 5 million unfractionated bone marrow cells from the primary recipients of 20 HSCs transplantations into lethally irradiated CD45.1 secondary recipient mice. Secondary peripheral blood multiple-lineage reconstitution was assessed from 4 weeks after transplantation. Limiting dilution assays comparing Hdc-GFP^{hi} and Hdc-GFP^{lo} HSCs were performed by analyzing recipient groups to which 20 or 50 HSCs were transplanted. HSC frequencies of non-responders were calculated using the criterion of < 1% donor contribution.

Hematopoietic stem cells and progenitors colony-forming assay

Bulk or single cells were sorted into methylcellulose culture medium (Stemcell Technology). Myeloid colony-forming capacity was assessed by MethoCult™ GF M3534 for myeloid committed progenitors. HSC colony-forming capacity was tested by using MethoCult™ GF M3434. HSPC Pre-B colony formation was modified by supplementing MethoCult™ M3630 medium with recombinant mouse IL-7 (BioLegend) and SCF (BioLegend) as described previously.

In vivo treatments

Mouse recombinant IFN-γ (BioLegend), IL-6 (BioLegend), and IL-7 (BioLegend) were injected intravenously at 5 μg/mouse. LPS-EB (InvivoGen) was injected intravenously at 0.25 mg/kg body weight. BM and spleen cells were harvested from LPS-challenged mice at 24 hours. In BrdU incorporation experiments, 1mg of BrdU (BD Biosciences) per 6 g body weight was injected intraperitoneally to either Hdc-GFP or *Hdc*$^{-/-}$; Hdc-GFP mice. BrdU incorporation was detected 14 hours after injection by using the BD Biosciences BrdU flow kit. For sepsis injury protection experiments, the H_2 agonist dimaprit dihydrochloride (Tocris Bioscience) was intraperitoneally injected twice a day for 5 consecutive days after 0.5 mg/kg LPS injection. For myeloid depletion experiments, 250 ng DT (List Biological Labs) was injected intraperitoneally every other day for one week. DT injections combined with a tamoxifen chow (Harlan Laboratories) regimen, was applied to deplete Hdc^{+} myeloid cells in Hdc-CreER^{T2}; tdTomato; iDTR mice. In some Hdc-DTR groups, 6 millions of *Hdc*$^{+/+}$; Hdc-GFP^{hi} or *Hdc*$^{-/-}$; Hdc-GFP^{hi}CD11b^{+}Gr1^{+} myeloid cells were transferred one day after DT treatment. For Gr1^{+} myeloid depletion, Hdc-GFP mice were injected intravenously 100μg anti-Gr1 (RB6-8C5, BioLegend) or rat IgG2b control (RTK4530, BioLegend) daily for 3 days. 5-FU (Sigma) was diluted in PBS and injected intravenously at 250 mg/kg. Bone marrow and blood were sampled from *Hdc*$^{-/-}$ and WT mice at 5 days. In irradiation protection experiments, 100 μg/mouse H_2 agonist or PBS was injected twice per day for 10 consecutive days prior to irradiation.

Quantitative RT-PCR

Hematopoietic stem cells, progenitors, and myeloid cells were sorted directly into the lysis buffer supplied from either RNeasy Micro kit (QIAGEN) or ARCTURUS PicoPure RNA isolation kit (Life Technologies). RNA was prepared following the manufacturer's instructions. cDNA was synthesized with a mixture of random and Oligo dT primers using SuperScript III Reverse Transcriptase (Life Technologies). Gene expression was determined using either PrimeTime qRT-PCR probe-based Assays (Integrated DNA Technologies) or FastStart Universal SYBR Green Assays (Roche Applied Science). Primers and probes sets for measuring cDNA expression include mouse Hdc (Mm.PT.58.41686379.g), H_1R (Mm.PT.58.42325479, Mm.PT.58.41154457, and Mm.PT.58.43886611), H_2R (Mm.PT.58.31195142), H_3R (Mm.PT.58.32340939), H_4R (Mm.PT.58.5634810) and Hprt (Mm.PT.58.32092191). Primer sequences of SYBR Green PCR assays are listed in Table S1. Quantitative PCR was performed with the Applied Biosystems Prism 9700 PCR machine. Relative gene expression was normalized to either Hprt or Gapdh.

RNA-seq analysis

Sorted HSCs (500 of each Hdc-GFP^{hi} or Hdc-GFP^{lo}) and HSPCs (2000 of each Hdc-GFP^{hi} or Hdc-GFP^{lo}, or 2000 of each WT or Hdc−/−) were lysed in RNA lysis buffer supplied in ARCTURUS PicoPure RNA isolation kit (Life Technologies). Total RNA was isolated in accordance with manufacturer's protocol. cDNA was amplified, and libraries were constructed by using SMARTer Ultra Low Input RNA Kit (Clontech Laboratories) and Nextera XT DNA Library Preparation Kit (Illumina) according to the respective manufacturer's instructions. Sequencing was performed with Hiseq 2500 (Illumina).

Microarray gene expression profiling

Fractions of bone marrow myeloid cells were isolated from Hdc-GFP mice long bones by flow sorting using combinations of myeloid cell surface makers including CD11b, Gr1, and GFP. Total mRNA was purified by using RNeasy Micro kit (QIAGEN) according to the manufacturer's instructions. RNA was labeled by using the 3′ IVT Expression Kit before hybridized to the Affymetrix GeneChip mouse genome 430 2.0 array. Arrays were scanned on an Affymetrix Scanner 3000-7G scanner with GCOS software.

Cell culture and protein detection

Prepared bone marrow stromal cells were washed and passed through a 70 μm nylon mesh to get single layer cells. Cells were then rinsed and plated in Minimum Essential Media (GIBCO) supplemented with 20% fetal bovine serum and 1% penicillin and streptomycin (GIBCO). Cells were passed three times over 17 days to enrich and expand adhesive stromal cells. Sorted GFP^{hi} or GFP^{lo} fractions of Lin^{-}c-kit^{+}Sca-1^{+} HSPCs were added and cultured for an additional 7-10 days. In some groups, histamine (Tocris Bioscience), H_2 agonist, or the H_2 antagonist ICI 162,846 (Tocris Bioscience) were added. For triple cultures, CD11b^{+}Gr1^{hi} myeloid cells (GFP^{+} or GFP^{-}) were added along with HSPCs. After culturing, Hdc-GFP^{hi} cells were recorded, counted, and flow analyzed by combinations of hematopoietic cell surface markers. For analyzing the HSPC cell cycle after culturing, HSPCs were sorted, fixed and permeablized

before being stained with Ki67 and Hoechst 33342. In HSCs stability assays, 4×10^3 Hdc-GFP^{hi} HSCs were harvested from the BM of Hdc-GFP mice and seeded into RPMI1640 with 20% FBS, 50 ng/ml recombinant mouse SCF, 10 ng/ml recombinant mouse IL-3, and 10 ng/ml recombinant mouse IL-6. After cultured for 5 days, the cells were analyzed with the same templates used in sorting. LPS treatment experiments, fractions of HSCs and CD11b$^+$Gr1$^+$ myeloid cells were sorted into X-VIVO™ 15 medium. SCF and TPO (both from BioLegend) were added to HSC culture at 50 ng/ml concentration. 10 ng/ml GM-CSF (BioLegend) was added to the myeloid cell culture. LPS (1 μg/ml, LPS-EB Ultrapure, InvivoGen) was added 12 hours after cells were plated. The supernatant was collected 6 hours after LPS treatment. In some experiments, mouse femur cell-free bone marrow supernatant was collected. Proteins from serum or bone marrow supernatant were measured by using ELISA Kit (Histamine: Enzo Life Science; IL6, IL7, and IFN-γ: Thermo Fisher Scientific) according to manufacturer's protocol.

Immunofluorescence microscopy

Dissected mouse femora and spleen were fixed in 4% PFA, embedded in OCT, and snap frozen in liquid nitrogen. Bones were sectioned using CryoJane Tape-Transfer system (Leica Biosystems). Slides were permeabilized with 0.5% Triton X-100 in PBS and blocked with blocking buffer. Primary antibodies were applied for overnight staining. AlexaFluor secondary antibodies (Invitrogen) were used to reveal the staining. All slides were counterstained and mounted with ProLong anti-fade mounting medium (Invitrogen). Images were acquired with an A1 laser scanning confocal attachment on an Eclipse Ti microscope stand (Nikon Instruments, Melville, NY).

Reproducibility

Experimental results were replicated at least once, unless otherwise indicated. Sample sizes for each study were estimated on the basis of the expected differences and previous experience with the particular assay. Power calculations were performed when needed. In most cases, studies were performed on genotype positive litters, with genotype negative litters used as controls. Blinding was not deemed to be required for most studies.

QUANTIFICATION AND STATISTICAL ANALYSIS

Statistical analysis was performed to detect the significance of differences in means of the abundance of mRNA or cell types, or of survival, in the different conditions being compared. All data are shown as the mean ± SEM. Kaplan-Meier survival was statistically analyzed by Logrank test. Other statistical comparisons were evaluated with Student's t test or one-way ANOVA. Statistical analysis was performed using Prism 7 (Graphpad). Significance levels were set at $^*p < 0.05$; $^{**}p < 0.01$; $^{***}p < 0.001$; n.s., not significant. n.d., not detectable. n indicates biological replicates. For each experiment the specific statistical details can be found in the figure legends.

Gene expression microarray analysis

A battery of quality test was performed to test the quality of the arrays. Samples were normalized using the GCRMA algorithm, and the statistical significance of differential expression was estimated using Linear Models for MicroArrays (Limma). A significance cutoff of a Benjamini-Hochberg false discovery rate, fdr $\leq$ 0.05 was used (Benjamini and Hochberg, 1995). This analysis was performed using the Bioconductor platform in the R statistical computing environment.

Analysis of RNA-seq data

30M single-end reads per sample were taken. Sequenced reads were mapped to the NCBI annotated genes of the mm9 assembly of the mouse genome with BowTie2 and TopHat 2.0.4. Expression datasets are available in Gene Expression Omnibus (GEO). The statistical significance of differential expression was estimated with weighted Limma-Voom for HPSCs or Deseq2 for HSCs both of which run under Bioconductor/R. A significance cutoff of fdr $\leq$ 0.05 was used, except specifically mentioned otherwise. Significantly differentially expressed genes (fdr $\leq$ 0.05 and absolute value of $\log_2$ fold change $\geq$ 0.6, were assigned to Biological Process Gene Ontology (GO) categories and KEGG pathways with iPathwayGuide. GO categories and pathways relevant to biological processes under discussion were chosen for further investigation.

Computational modeling of HSC distribution

MB-HSC was identified by GFP$^+$CD150$^+$Lin$^-$CD41$^-$CD48$^-$ (represented as "yellow" cells, since they stain for green (GFP), and red (CD150), but not blue (Lineage, CD41, CD48) on Hdc-GFP mouse bone sections. Next, an MB-HSC/myeloid cluster was defined by the presence of direct contact between an MB-HSC with at least 2 GFP$^+$CD150$^-$ myeloid cells. All MB-HSCs found in a given section were scored and marked using the Fiji distribution of ImageJ, and the percentage of such MB-HSCs that were present in MB-HSC/myeloid clusters was calculated. To assess whether the observed cluster localization could have occurred by chance we used methods similar to those in previously published work (Bruns et al., 2014; Cordeiro Gomes et al., 2016). Simulated images were generated using an ImageJ Python script (available from https://github.com/theresaswayne/random-cells). For each confocal image field analyzed, spots were placed randomly on the tissue area in the CD150 (red) channel and overlaid on the GFP channel. The size and density (number per μm^2) of the randomized spots were set to match the size and density of observed MB-HSCs in the original

image. The spots were also constrained not to overlap with each other. These simulated images were then scored for their co-location within the above mentioned ''cluster.'' In total, 2480 random spots and 541 MB-HSCs were analyzed.

DATA AND SOFTWARE AVAILABILITY

Microarray data have been deposited in the Gene Expression Omnibus (GEO) under the following accession numbers: Hdc-GFP^{hi}CD11b^{+}Gr1^{+} and Hdc-GFP^{lo}CD11b^{+}Gr1^{+} cells (GEO: GSE79728) and for Hdc-GFP^{hi}CD11b^{+}Gr1^{hi} and Hdc-GFP^{hi}CD11b^{+}Gr1^{lo} cells (GEO: GSE80143). RNA-Seq data has been deposited in the GEO under the following accession numbers: Hdc-GFP^{hi} HSCs and Hdc-GFP^{lo} HSCs (GEO: GSE90787), Hdc-GFP^{hi} HSPCs and Hdc-GFP^{lo} HSPCs (GEO: GSE80092), and *Hdc*$^{-/-}$ HSPCs and WT HSPCs (GEO: GSE80284).